Minimizing aerosol effects on the OMI tropospheric NO_2 retrieval – An improved use of the 477 nm O_2-O_2 band and an estimation of the aerosol correction uncertainty

Julien Chimot[1,a], J. Pepijn Veefkind[1,2], Johan F. de Haan[2], Piet Stammes[2], and Pieternel F. Levelt[1,2]

[1]Department of Geoscience and Remote Sensing (GRS), Civil Engineering and Geosciences, Delft University of Technology (TU Delft), the Netherlands

[2]Royal Netherlands Meteorological Institute, De Bilt, the Netherlands

[a]now at European Organisation for the Exploitation of Meteorological Satellites (EUMETSAT), Darmstadt, Germany

Correspondence to: Julien Chimot (Julien.Chimot@eumetsat.int)

Abstract. Global mapping of satellite tropospheric NO_2 vertical column density (VCD), a key gas in air quality monitoring, requires accurate retrievals over complex urban and industrialized areas and under any atmospheric conditions. The high abundance of aerosol particles in regions dominated by anthropogenic fossil fuel combustion, e.g. mega-cities, and/or biomass burning episodes affects the space-borne spectral measurement. Minimizing the tropospheric NO_2 VCD biases caused by aerosol scattering and absorption effects is one of the main challenges for the retrieval from air quality satellite instruments. In this study, reference Ozone Monitoring Instrument (OMI) DOMINO-v2 product was reprocessed over cloud-free scenes, by applying new aerosol correction parameters retrieved from the 477 nm O_2-O_2 band, over east China and South America for 2 years (2006-2007). These new parameters are based on two different and separate algorithms developed during the last two years in view of an improved use of the OMI 477 nm O_2-O_2 band: 1) the updated OMCLDO2 algorithm which derives improved effective cloud parameters, 2) the aerosol neural network (NN) which retrieves explicit aerosol parameters by assuming a more physical aerosol model. The OMI aerosol NN is a step ahead to OMCLDO2 by primarily estimating an explicit aerosol layer height (ALH), and secondly an aerosol optical thickness τ for cloud-free observations. Overall, it was found that all the considered aerosol correction parameters reduce the biases identified in DOMINO-v2 over scenes in China with high aerosol abundance dominated by fine scattering and weakly absorbing particles: e.g. from $[-20{:}-40]\%$ to $[0{:}20]\%$ in summertime. The use of the retrieved OMI aerosol parameters leads in general to a more explicit aerosol correction and higher tropospheric NO_2 VCD values, in the range of $[0{:}40]\%$, than from the implicit correction with the updated OMCLDO2. This number overall represents an estimation of the aerosol correction strategy uncertainty nowadays for tropospheric NO_2 VCD retrieval from space-borne visible measurements. The explicit aerosol correction theoretically includes a more realistic consideration of aerosol multiple scattering and absorption effects, especially over scenes dominated by strongly absorbing particles, where the correction based on OMCLDO2 seems to remain insufficient. However, the use of ALH and τ from the OMI NN aerosol algorithm is not a straightforward operation and future studies are required to identify the optimal methodology. For that purpose, several elements are recommended in this paper. Overall, we demonstrate the possibility to apply a more explicit aerosol correction by considering aerosol parameters directly derived from the 477 nm O_2-O_2 spectral band, measured

by the same satellite instrument. Such an approach can, in theory, easily be transposed to the new-generation of space-borne instruments (e.g. TROPOMI on-board Sentinel-5 Precursor), enabling a fast reprocessing of tropospheric NO_2 data over cloud-free scenes (cloudy pixels need to be filtered out), as well as for other trace gas retrievals (e.g. SO_2, HCHO).

1 Introduction

Long-time series of UV-visible (UV-vis) satellite measurements are a great asset for monitoring the distribution and evolution of pollutants such as NO_2, HCHO, or SO_2 and aerosol particles in the troposphere. With the forthcoming new generation of sensors like TROpospheric Ozone Monitoring Instrument (TROPOMI) on-board Sentinel-5-Precursor (Veefkind et al., 2012), Sentinel-4-UVN, and Sentinel-5-UVNS within the Copernicus program (Ingmann et al., 2012), they will become an important tool for verifying the effectiveness of implemented technology to protect environment and population against air pollution (Duncan et al., 2016). While the last generation of space instruments have had a pixel size between 13 x 24 km^2 for the Ozone Monitoring Instrument (OMI) or 80 x 40 km^2 for the Global Ozone Monitoring Experiment (GOME-2), the new generation has smaller pixel sizes (about 7 x 3.5 km^2 for TROPOMI), allowing air quality mapping of complex urban and city areas. This is also expected to reduce the probability of cloud contamination. However, the significant probability of aerosol contamination in areas such as India, China or regions dominated by biomass burning episodes will likely remain, or may even increase.

OMI is the Dutch Finnish push-broom spectrometer flying on the National Aeronautics and Space Administration (NASA)'s Earth Observation Satellite (EOS)-Aura platform since July, 15th 2004. Its Sun-synchroneous orbit has a local equator crossing-time of approximately 13:40h. Operational tropospheric NO_2 product derived from the visible backscattered spectral light (405-465 nm), such as the OMI DOMINO-v2 (Boersma et al., 2011) or the very recent Quality Assurance for Essential Climate Variables (QA4ECV), is nowadays a reference. The related global mapping of tropospheric NO_2 concentrations has been used by many air quality research studies focusing on NO_x emissions, secondary pollutant formation, as well as tropospheric NO_x chemistry and transport: e.g. (Curier et al., 2014; Reuter et al., 2014; Ding et al., 2015).

A critical element for an accurate tropospheric NO_2 vertical column density (VCD) retrieval is our capability to reproduce the average light path along which the photons travelled before being detected by the satellite sensor at the top of the atmosphere (TOA) in the visible spectral window. In particular, scattering and absorption induced by atmospheric aerosol particles over cloud-free scenes are known to lead to very complex light path. Because they are emitted by the same sources, high NO_2 and aerosol concentrations are often spatially correlated (Veefkind et al., 2011). Therefore, aerosol contamination needs to be properly addressed in the retrieval algorithms. In the frame of tropospheric NO_2 retrievals from visible spectral measurements based the differential optical absorption spectroscopy (DOAS) approach, the aerosol correction has to be applied on the air mass factor (AMF): a unitless number representative of the length of the average light path.

Over cloud-free scenes, a full explicit aerosol correction ideally requires a comprehensive set of parameters describing aerosols: i.e. the single scattering albedo ω_0, scattering phase function, load through the aerosol optical thickness (AOT) τ, size, and vertical distribution (Martin et al., 2003; Leitão et al., 2010; Bousserez, 2014). Among all these variables, many studies emphasized the importance of the aerosol layer height (ALH) knowledge (Leitão et al., 2010; Castellanos et al., 2015;

Chimot et al., 2016). Assuming no aerosol correction, i.e. aerosol-free scene (Richter and Burrows, 2002), would clearly create large biases on the OMI tropospheric NO_2 retrievals (Chimot et al., 2016).

There are basically two strategies for achieving the aerosol correction in the AMF: 1) either by considering external data, or 2) by using the available particle parameters that can be simultaneously derived from the same UV-visible spectral space-borne measurement. Studies that reprocessed DOMINO-v2 dataset using external data usually relied either on atmospheric transport model outputs, e.g. GEOS-Chem in the Peking University OMI NO_2 (POMINO) (Lin et al., 2014, 2015), or observations issued from different satellite platforms, e.g. the Cloud-Aerosol Lidar with Orthogonal Polarization (CALIOP) (Castellanos et al., 2015), or even both combined together (Liu et al., 2018). Resulting changes mostly occurred in case of high aerosol pollution (τ(550 nm) > 0.8) with increased or decreased tropospheric NO_2 VCDs depending on the geophysical conditions and aerosol properties and distributions. However, the resulting AMF computation becomes dependent on these data sources, their quality and the possibility (or not) to combine them altogether. In general, spatial and temporal co-registration between the different instruments or due to different resolution between the observation pixel and the model grid cell may become an issue. In the frame of an operational processing, it is generally preferred to maximize the exploitation of the spectral measurement acquired by a same instrument representative of the considered observation pixel. One of the main reasons is the need to have an indication on particle height representative of the average light path associated with every single OMI field of view (FOV). Such an information is generally not easily and directly available from an external source. Exploitation of the 477 nm O_2-O_2 absorption for aerosol retrieval is very promising. It is not only measured by OMI, but also by GOME-2, TROPOMI, Sentinel-4-UVN and Sentinel-5-UVNS. Several studies based on ground-based and satellite instrument have demonstrated its relative high sensitivity to aerosols, in particular to ALH (Wagner et al., 2004; Castellanos et al., 2015; Park et al., 2016; Chimot et al., 2016, 2017).

Because of the difficulty to easily distinguish clouds from aerosols, and to identify the right aerosol model to use, it has always been preferred to retrieve effective clouds assuming a Lambertian and opaque reflector model (Joiner et al., 2004; Acarreta et al., 2004; Stammes et al., 2008; Vasilkov et al., 2018) and consequently to compute the resulting troposphere NO_2 AMF for all the OMI scenes, regardless of the type of particles present in the scene (clouds and/or aerosols). Such a correction is historically named an "implicit aerosol correction" (Boersma et al., 2004, 2011). Chimot et al. (2016) clearly demonstrated that, in spite of its implicit nature, the implicit aerosol correction mitigates biases on the OMI DOMINO NO_2 product over cloud-free scenes compared to an aerosol-free pixel assumption. However, limitations were identified: 1) a numerical artifact is present due to a too coarse sampling employed in the OMI cloud look-up-table (LUT) leading then to a strong underestimation on the OMI tropospheric NO_2 VCD over scenes with τ(550 nm) $\geq$ 0.6 and aerosols located at high altitude, 2) the Lambertian cloud model, in spite of its benefits, remains somehow too simple and likely does not fully reproduce all the multiple scattering effects inherent to aerosol properties. The OMI effective cloud algorithm was then updated in order to remove these numerical artifacts (Veefkind et al., 2016). It also includes many additional relevant improvements related to the OMI 477 nm O_2-O_2 measurement. But its impact on the correction for aerosols has not yet been evaluated.

To move one step further, Chimot et al. (2017) developed a novel machine learning algorithm, based on the neural network (NN) technique, that allows to retrieve ALH together with τ from the same OMI 477 nm O_2-O_2 spectral band over cloud-

free scenes. These retrievals were performed on various cases both over land and sea and compared with reference CALIOP observations and related climatology (Chimot et al., 2017, 2018). They benefit from a strong synergy with MODIS on-board the NASA Aqua platform flying together with Aura in the same NASA A-Train constellation, in order to identify the cloud-free scenes and to better constrain the ALH retrieval quality. For such a purpose, the 477 nm O_2-O_2 band represents some advantages compared to the more traditional O_2-A band at 760 nm which is not measured by OMI: 1) it is spectrally closer to the NO_2, HCHO, or SO_2 absorption features, 2) it has a wider spectral range although weaker signal leading to high sensitivities in case of high aerosol loading, and 3) it has less radiative transfer challenges arising from strong absorption lines like in the near-infrared. Moreover, the NN technique development allows a very fast OMI data processing which is an important requirement within an operational environment. The aerosol retrievals performed with this algorithm are expected to lead to an explicit aerosol correction over cloud-free scenes by using the OMI 477 nm O_2-O_2 measurement simultaneously acquired with the 405-465 nm NO_2 band.

This paper aims to evaluate the benefits of our improved use of the OMI 477 nm O_2-O_2 band for correcting aerosol effects in tropospheric NO_2 VCD retrieval from the same visible observation. We evaluate the potential of directly using the OMI NN aerosol ALH (and τ) in view of an explicit correction. We also assess the expected changes in the implicit aerosol correction based on the improved OMI effective cloud algorithm. To compare the different aerosol correction strategies, we reprocessed 2 years (2006-2007) of the DOMINO-v2 data over different areas and seasons, dominated by different types of pollution episodes and thus, NO_2 and aerosol sources: 1) the large urban and industrialized east China region dominated by a mix of continental polluted fine and weakly absorbing particles, and dust coarse and scattering particles in summer time (June-July-August), 2) the same area essentially dominated by continental polluted fine and weakly absorbing particles in winter time (December-January-February), and 3) South America during the biomass burning season associated with heavy load of strongly absorbing aerosol emission (August-September). Given all the aerosol corrections available from on our improved use of the OMI 477 nm O_2-O_2 band, their comparison in this paper gives an estimation of the aerosol correction uncertainty in the OMI tropospheric NO_2 VCD retrieval. Sections 2 and 3 describe the algorithms and the reprocessing methodology. Section 4 evaluates the results of the applied aerosol corrections in the reprocessed tropospheric NO_2 retrievals. To complete the analyses, Sect. 5 includes specific discussions based on reference simulations to better understand the behaviour of the new OMI tropospheric NO_2 VCD. Similarly to Chimot et al. (2016), the advantage of such simulations is to determine, on well controlled cases, the expected new biases of the reprocessed OMI tropospheric NO_2 VCD and to identify the key geophysical factors driving them. At the end, in Sect. 6, we discuss about the benefits and challenges of each aerosol correction.

2 The OMI $O_2 - O_2$ algorithms

2.1 $O_2 - O_2$ DOAS spectral fit

In this paper, both effective cloud and aerosol algorithms are based on the same OMI 477 nm $O_2 - O_2$ spectral band. More specifically, they use the continuum reflectance R_c(475 nm) and the O_2-O_2 slant column density (SCD) $N^s_{O_2-O_2}$. These

variables are derived from the DOAS spectral fit approach, which is then a prerequisite before applying either the OMI cloud look-up-table (LUT) (see Sect. 2.2) or the aerosol neural networks (see Sect. 2.3).

The DOAS method is a specific spectral fit approach following basic principle of absorption spectroscopy employed for UV and visible absorbing trace gases. The various DOAS techniques rely on the same key concept: a simultaneous fit of several trace gas slant column densities from the fine spectral features due to their absorption (i.e. the high frequency part) present in passive UV–visible spectral measurements of atmospheric radiation (Platt and Stutz, 2008). The assumed Beer-Lambert (or Bouguer-Lambert) law describes the light attenuation as a function of the travelled distance in the atmosphere, gas concentration and its spectral absorption intensity. It is commonly employed for absorption spectroscopy analyses of NO_2, SO_2, HCHO and O_3 from the OMI, TROPOMI, GOME, GOME-2 and SCIAMACHY sensors: e.g. (Boersma et al., 2011; De Smedt et al., 2017). The spectral fit is achieved within a predefined spectral window and the slant column density N^{s} is defined as the column density of a trace gas absorber along the average light path travelled by the detected photons from the Sun through the atmosphere, surface and back to the satellite sensor.

Here, the OMI 477 nm O_2-O_2 DOAS fits together the absorption cross-section spectrum of O_2-O_2 with a first-order polynomial over the (460–490 nm) spectral band (Acarreta et al., 2004; Veefkind et al., 2016). Note that the O_3 absorption, also present in this band, is taken into account. The continuum reflectance R_{c} at the reference wavelength λ_0 = 475 nm is the reflectance which would be measured in the absence of O_2-O_2 in the atmosphere.

In the absence of clouds, both OMCLDO2 and OMI aerosol algorithms rely on how aerosols affect the length of the average light path along which O_2-O_2 absorbs. R_{c}(475 nm) is known to represent the enhanced scene brightness due to the additional scattering effects induced by the particles. In particular, R_{c}(475 nm) directly increases with increasing τ. The enhancement magnitude however depends on aerosol properties as well as the surface albedo (Boersma et al., 2011; Chimot et al., 2016; Castellanos et al., 2015). $N^{\mathrm{s}}_{\mathrm{O_2-O_2}}$ is governed by the overall shielding or enhancement effect of the absorption of the photons by the O_2-O_2 complex in the visible spectral range along the average light path. A reduction of the length of the average light path, i.e. shielding effect, reduces the absorption by O_2-O_2. The aerosol layer height is the primary driver (Castellanos et al., 2015; Chimot et al., 2016, 2017). An aerosol layer located at high altitudes causes a large shielding effect on the O_2-O_2 located in the atmospheric layers below, by reducing the amount of photons coming from the top-of-atmosphere and reaching the lowest part of the atmosphere, compared to an aerosol-free scene. As a second order effect, aerosol properties such as τ and ω_0, and surface reflectance also contribute to $N^{\mathrm{s}}_{\mathrm{O_2-O_2}}$ (Castellanos et al., 2015; Chimot et al., 2016, 2017).

2.2 OMI cloud algorithm OMCLDO2

The OMI cloud algorithm also named OMCLDO2 (Acarreta et al., 2004) derives the effective cloud fraction c_f and cloud pressure c_p assuming a single cloud layer as an opaque Lambertian reflector with a constant albedo of 0.8 (Stammes et al., 2008) and the independent pixel approximation (IPA) (Martin et al., 2002; Acarreta et al., 2004). The measured reflectance R is formulated as a linear combination of a clear-sky R_{Clear} and a cloudy reflectance R_{Cloud} (Martin et al., 2002; Acarreta

et al., 2004):

$$R(\lambda) = \mathrm{c}_f \cdot \mathrm{R}_{Cloud} + (1 - \mathrm{c}_f) \cdot \mathrm{R}_{Clear}. \quad (1)$$

A look-up-table (LUT) enables the conversion of R_{c}(475 nm) and $N^{\mathrm{s}}_{\mathrm{O_2}-O_2}$ into c_f and c_p. It requires knowledge on the surface reflectance and surface pressure in addition to the viewing and sun geometry configurations (Acarreta et al., 2004; Veefkind et al., 2016). Because of the low impact of small clouds on the O_2-O_2 band, c_p has large uncertainties in case of low c_f (Acarreta et al., 2004). The term "effective" here means that these cloud parameters do not represent actual clouds, but our best explanation of the measured radiance by combining these variables with the assumed approximate model (Sneep et al., 2008; Stammes et al., 2008). Therefore, the retrieved c_f and c_p values of each observed scene match with the measurement summarized by (R_{c}(475 nm)- $N^{\mathrm{s}}_{\mathrm{O_2}-O_2}$), such that the (460–490 nm) radiance budget is comprehensively closed (apart from instrument noise). For example, true optically thin clouds will be retrieved as a an opaque and bright Lambertian reflector covering only a small part of the OMI pixel, mostly because of the large assumed cloud albedo value (Veefkind et al., 2016).

The main motivation of this cloud retrieval scheme has been the correction of cloud effects in trace gas retrievals (Stammes et al., 2008). However, this algorithm is actually applied both to cloudy and cloud-free scenes with aerosols, without any prior distinction. Many studies demonstrated that OMCLDO2 accounts for a large part of aerosol effects in the retrieved c_f and c_p (Boersma et al., 2004, 2011; Castellanos et al., 2015; Chimot et al., 2016; Wang et al., 2015). Under these conditions, the OMI cloud parameters become then "more effective" as they do not represent anymore cloud but aerosol effects on the (460–490 nm) radiance. One could claim that OMCLDO2 becomes then an approximate aerosol model, independent of those considered in Sect. 2.3. Chimot et al. (2016) demonstrated how OMCLDO2 responses to aerosols: 1) c_f is mostly driven by R_{c}(475 nm) and increases with increasing aerosol load, regardless of its altitude. Its magnitude is weighted by aerosol properties and surface conditions. 2) c_p represents beforehand the degree of shielding effect applied by aerosols, which results from a complex combination of ALH as a first order, aerosol load τ and type, surface properties and geometry angles as a second order. A stronger shielding effect leads to a lower c_p. In general, over scenes with high τ values, c_p correlates well with ALH. Furthermore, regardless of true aerosol layer altitude, strongly absorbing particles lead to a decrease of c_p, while the presence of more scattering particles increases c_p values (Castellanos et al., 2015; Chimot et al., 2016).

Veefkind et al. (2016) released a new version of the OMCLDO2 product. The new algorithm, here named OMCLDO2-New, includes several improvements such as a better consistency of gas absorption cross sections with the OMI NO_2 retrieval algorithm, outlier removal from the spectral fitting, etc.. However, in the context of the implicit aerosol correction, the expected highest changes come from the higher number of nodes of the OMI cloud LUT. Indeed, the coarse sampling of the OMI cloud LUT associated with the OMCLDO2-Old version created a numerical artefact: c_p was increasing with decreasing c_f (or aerosol τ) without any physical explanation (Chimot et al., 2016; Veefkind et al., 2016). This has strong impacts in the OMI tropospheric NO_2 product, DOMINO v2, in scenes dominated by aerosols (see Sect. 3.3). Furthermore, a temperature correction is implemented in OMCLDO2-New to take into account the density squared dependence of the O_2-O_2 absorption. Its impact however depends on the temperature conditions and latitude area (Veefkind et al., 2016).

2.3 OMI aerosol neural network

The OMI O_2-O_2 aerosol algorithm relies on a NN multilayer perceptron approach to retrieve primarily ALH over cloud-free scenes, but also aerosol τ(550 nm) as a secondary parameter (Chimot et al., 2017, 2018). Since a fine characterization of aerosol vertical profiles cannot be retrieved from OMI UV-visible measurements, they are assumed as one box layer with a constant pressure thickness (100 hPa). ALH is the mid-altitude of this layer in km over sea level but can also be expressed in pressure. Here, the strategy differs from the OMI effective clouds of Sect. 2.2. The main motivation is to try to reproduce aerosol scattering and absorption in the visible spectrum via a more explicit aerosol model than the assumed opaque Lambertian reflector. Particle properties in this layer are considered to be homogeneous.

ALH retrieval requires several input variables, the most critical being τ(550 nm) as both ALH and τ(550 nm) similarly affect $N^{\mathrm{s}}_{\mathrm{O_2-O_2}}$ and need to be separated (Chimot et al., 2017). In theory, τ information may be available from diverse sources (e.g. atmospheric models, statiscal prior guess, or observations). In practice, MODIS τ product has systematically been preferred due to its good spatial and temporal collocation with OMI measurements, and its recognized high quality. Retrieved OMI τ may also be used as they come from a same spectral measurement (same instrument). However due to its higher uncertainty compared to MODIS, its use impacts the quality of OMI ALH (Chimot et al., 2017). For OMI τ retrieval, R_{c}(475 nm) is considered instead of τ as prior input. Note that in the next sections, we define NN_{MODIS} when prior MODIS τ is considered, NN_{OMI} based on the retrieved OMI τ, and NN_{True} when true τ value is considered for the synthetic cases (see Sect. 3.1).

The training data set was generated by full-physical spectral simulations, assuming explicit aerosol particles without clouds, and with the Determining Instrument Specifications and Analyzing Methods for Atmospheric Retrieval (DISAMAR) software of KNMI (de Haan, 2011). Aerosol scattering phase function $\Phi(\Theta)$ was simulated by the Henyey–Greenstein (HG) function parametrized by the asymmetry parameter g, the average of the cosine of the scattering angle (Hovenier and Hage, 1989). Aerosols were specified as standard fine particles with a typical value of the extinction Ångström exponent $\alpha = 1.5$ and $g = 0.7$. They are assumed to fully cover the OMI pixel. To take into account the inaccuracies of the assumed aerosol single scattering albedo ω_0 properties, two training data sets were generated with a different typical value: one with $\omega_0 = 0.95$ and one with $\omega_0 = 0.9$ in the visible spectral domain. Therefore, two separate OMI ALH NN algorithms were developed, one for each aerosol ω_0 values. The rational of these ω_0 values relies on those that are typically identified in the regions dominated by high NO_2 pollution, notably in east China (Lin et al., 2014, 2015).

The HG function is known to be smooth and reproduce the Mie scattering functions reasonably well with $g = 0.7$ for most of aerosol types (Dubovik et al., 2002). A similar approach is considered for the operational ALH retrieval algorithms for Sentinel-4 and Sentinel-5 Precursor (Leitão et al., 2010; Sanders et al., 2015; Colosimo et al., 2016; Nanda et al., 2017), and when applying various explicit aerosol corrections in the tropospheric NO_2 AMF calculation over urban and industrial areas dominated by anthropogenic pollution, for instance in east China (Spada et al., 2006; Wagner et al., 2007; Castellanos et al., 2015; Vlemmix et al., 2010).

Similarly to the high c_p inaccuracy in case of low c_f, high ALH bias is expected below a minimum particle load (i.e. threshold of τ(550 nm) = 0.5). This is directly due to the weak O_2-O_2 absorption within the 460-490 nm spectral band. Below

this threshold, low aerosol amounts eventually have negligible impacts on $N^{s}_{O_2-O_2}$. ALH retrieval performance was assessed over East China, South America, and Russia areas with scenes including urban, industrial, and biomass burning pollution events and for different seasons (Chimot et al., 2017, 2018). These scenes are mostly dominated by fine spherical particles, weakly absorbing (e.g. sulfate, and nitrate) or strongly absorbing (e.g. smoke). Dust particles may sometimes be mixed. Over cloud-free scenes, OMI ALH has shown consistent spatial patterns with CALIOP level 2 (L2) ALH over urban and industrial areas in east China, with an uncertainty in the range of [500:700] m and for collocated MODIS scenes with τ(550 nm) ≥ 0.5 (Chimot et al., 2018). Additional analyses showed that differences between the LIdar climatology of vertical Aerosol Structure for space-based lidar simulation (LIVAS) and 3-year OMI ALH with MODIS $\tau(550m) \geq 1.0$ were in the range of [180:800] m (Amiridis et al., 2015; Chimot et al., 2017). Finally, Chimot et al. (2018) showed the potential of OMI visible measurements to observe the height of thick and absorbing aerosol layers released by widespread fire episodes such as in South America. The aerosol model assumptions, in particular ω_0, are the most critical as they may affect ALH retrieval uncertainty up to a maximum of 660 m. An accuracy of 0.2 is necessary on prior τ(550 nm) information to limit ALH bias close to zero over scenes with τ(550 nm) $\geq$ 1.0, and below 500 m for τ(550 nm) values smaller than 1.0. A summary of all the OMI NN aerosol algorithms as well as related input and output parameters is given in Tab. 1.

3 From aerosol impacts to aerosol correction – Methodology

3.1 General methodology

Reprocessing of the OMI tropospheric NO_2 product is based on the DOMINO-v2 dataset (see Sect. 3.3) in which the AMF (see Sect. 3.2) is recomputed with diverse aerosol correction strategies using the DISAMAR radiative transfer model, over cloud-free scenes contaminated by aerosols. Recomputed AMF values replace then the original ones in DOMINO. They are applied to the available NO_2 SCD to derive consequently the tropospheric NO_2 VCD. Tropospheric NO_2 AMF computation follows the formulation detailed in Sect. 3.2 which relies either on an implicit or an explicit aerosol correction: the implicit correction considers the effective cloud retrievals obtained from OMCLDO2 (cf. Sect. 2.2); the explicit aerosol correction employs aerosol parameters: either OMI ALH and OMI τ from the OMI aerosol NN (cf. Sect. 2.3), or OMI ALH and MODIS τ. The complementary aerosol parameters (i.e. ω_o, g, α) follow those specified in the associated training dataset.

The surface albedo is based on the OMI Lambertian Equivalent Reflectivity (LER) climatology (Kleipool et al., 2008). In DOMINO-v2, this climatology is derived from a 3-year OMI time series measurements. However, it evolved since then with an extended 5-year OMI time series (Veefkind et al., 2016). This evolved OMI LER is considered for all the reprocessed tropospheric NO_2 VCD of this study. All the other geophysical parameters associated with DOMINO-v2, such as the NO_2 vertical profile, remain identical.

To identify cloud-free OMI observation pixels with aerosols, a similar strategy as Chimot et al. (2016, 2017) is considered. The DOMINO-v2 NO_2 scenes are collected together with the MODIS-Aqua aerosol τ(550 nm) from the combined Dark Target (DT) and Deep Blue (DB) product of Collection 6 available at the resolution of 10 km (Levy et al., 2013). They are collocated within a distance of 15 km. The probability of cloud-free OMI scene is a priori ensured by the availability of the MODIS

aerosol product with the highest quality assurance flag. In such a case, MODIS Aqua τ was then exclusively retrieved when a sufficient high amount of cloud-free sub-pixels was available (i.e. at the MODIS measurement resolution of 1 km) (Levy et al., 2013). However, it is well recognized this may be not completely representative for the atmospheric situation of the OMI pixel. Therefore, we added two thresholds for each collocated OMI-MODIS pixel: the geometric MODIS cloud fraction to be smaller than 0.1, and OMI c_f lower than 0.1. Past experiences showed that OMI c_f values in the range of [0.1:0.2] may still contain clouds (or both clouds and aerosols) (Boersma et al., 2011; Chimot et al., 2016).

Additional synthetic cases analysed in Sect. 4 and 5 are also based on the DISAMAR model, specified in a similar way as the NN training dataset in Sect. 2.3. Either OMCLDO2 or the OMI NN aerosol algorithms are used to determine the expected tropospheric NO_2 VCD biases.

3.2 Air mass factor computations

The computation of tropospheric NO_2 AMF $A^{\mathrm{v}}_{\mathrm{NO_2}}$ is a key step for converting NO_2 SCD $N^{\mathrm{s}}_{\mathrm{NO_2}}$ into tropospheric NO_2 VCD $N^{\mathrm{v}}_{\mathrm{NO_2}}$, which represents the number of NO_2 molecules cm^{-2} integrated along the vertical direction from the surface P_0 to the tropopause P_{trop} pressure. The application of $A^{\mathrm{v}}_{\mathrm{NO_2}}$ is crucial to correct of the average light path variability contained in $N^{\mathrm{s}}_{\mathrm{NO_2}}$. $A^{\mathrm{v}}_{\mathrm{NO_2}}$ computation has generally been recognized as the principal source of errors in $N^{\mathrm{v}}_{\mathrm{NO_2}}$ determination in areas with a high level of air pollution (Boersma et al., 2007). This was even more emphasized by Lorente et al. (2017) who discussed how AMF structural uncertainty is driven by assumed prior information, and cloud and aerosol correction strategies: up to 42% over polluted regions, and 31% over unpolluted regions.

In the context of OMI visible spectral measurements, $A^{\mathrm{v}}_{\mathrm{NO_2}}$ is defined as the ratio of the atmospheric SCD and VCD (Boersma et al., 2011):

$$A^{\mathrm{v}}_{\mathrm{NO_2}}(\Psi,\lambda) = N^{\mathrm{s}}_{\mathrm{NO_2}}(\Psi,\lambda)/N^{\mathrm{v}}_{\mathrm{NO_2}}, \tag{2}$$

with Ψ the list of input parameters prerequisite for the radiative transfer model. Note that before performing this conversion, the stratospheric and tropospheric contributions to $N^{\mathrm{s}}_{\mathrm{NO_2}}$ must be separated. Therefore, $A^{\mathrm{v}}_{\mathrm{NO_2}}(\Psi,\lambda)$ is only applied to the tropospheric NO_2 SCD. The OMI $A^{\mathrm{v}}_{\mathrm{NO_2}}$ formulation follows Palmer et al. (2001); Boersma et al. (2004) and the concept of altitude-resolved AMF $a(z)$ (also named block AMF or BAMF) introduced by Palmer et al. (2001); Eskes and Boersma (2003), and then generalised by Wagner et al. (2007); Rozanov and Rozanov (2010); Richter and Wagner (2011). The ratio of a to the total air mass factor $A_{\mathrm{NO_2}}$ (deduced from the NO_2 shape profile) gives the vertical averaging kernel AK: i.e. the sensitivity of the satellite measurement to each vertical atmospheric layer (Eskes and Boersma, 2003; Richter and Wagner, 2011). Overall, $A^{\mathrm{v}}_{\mathrm{NO_2}}$ can then be seen as a unitless number representative of the length of the average light path followed by the detected photons in the troposphere. It includes then an indication about the sensitivity to the amount of NO_2 in the troposphere, larger values indicating a higher sensitivity assuming no change in vertical NO_2 profile. Indeed, in those cases, a change in $A^{\mathrm{v}}_{\mathrm{NO_2}}$ is directly associated with a change of a at the atmospheric levels where the trace gas is present. The reference wavelength considered in this paper is 439 nm, following the OMI NO_2 product (see Sect. 3.3) (Boersma et al., 2011).

Aerosols may cause either a shielding or an enhancement effect. A shielding effect occurs when the length of the average light path is reduced leading then to a decrease of $A^{\mathrm{v}}_{\mathrm{NO_2}}$. Reciprocally, an enhancement affect results in an increase of $A^{\mathrm{v}}_{\mathrm{NO_2}}$ (Leitão et al., 2010; Chimot et al., 2016). Following Eq. 2, any bias in $A^{\mathrm{v}}_{\mathrm{NO_2}}$ calculation leads to a direct bias into $N^{\mathrm{v}}_{\mathrm{NO_2}}$: same value but opposite sign.

Note that in the case of real OMI tropospheric NO_2 retrievals, a temperature correction is often applied as the temperature of the assumed NO_2 absorption cross section, fixed at 221 K, can differ from the actual temperature when deriving $N^{\mathrm{s}}_{\mathrm{NO_2}}$. The correction term is thus implemented in the computation of $A^{\mathrm{v}}_{\mathrm{NO_2}}$ such that it represents the ratio of $N^{\mathrm{s}}_{\mathrm{NO_2}}$ derived with a NO_2 cross section at the real temperature T to the column derived at 221 K. European Centre for Medium-Range Weather Forecasts (ECMWF) temperature fields are used for this correction (Boersma et al., 2004, 2011).

Computation of $A^{\mathrm{v}}_{\mathrm{NO_2}}$ requires accurate knowledge about all the parameters Ψ affecting the optical properties of the atmosphere and the length of the average light path. For an aerosol and cloud-free scene, Ψ generally includes the satellite and solar geometries, ground-pressure and the surface reflectance. In the presence of clouds and/or aerosols, adequate parameters describing their properties must be added. Among all these variables, many studies emphasized that ALH and τ are the most critical aerosol parameters affecting primarily $A^{\mathrm{v}}_{\mathrm{NO_2}}$ over cloud-free scenes dominated by aerosol particles (Leitão et al., 2010; Castellanos et al., 2015; Chimot et al., 2016). It was clearly demonstrated that other parameters describing aerosol properties, such as size, are generally of second order of magnitude for such a purpose. The main reason is because to correct of aerosol effects, we overall need the length of the average light path in presence of scattering and absorbing particles. This is primarily driven by τ and ALH (in addition to the shape of the NO_2 vertical profile), much less by the detailed properties of particles that affect more the TOA radiance measurement (Chimot et al., 2016).

3.3 OMI tropospheric NO_2 dataset – DOMINO v2

DOMINO v2 (Boersma et al., 2011) is a reference worldwide tropospheric NO_2 product derived from the OMI visible measurements and can be downloaded from the Tropospheric Emissions Monitoring Internet Service (TEMIS) website (http: www.temis.nl). Chimot et al. (2016) demonstrated that the implicit aerosol correction in DOMINO-v2 is better than the clear-sky assumption (Richter and Burrows, 2002)), with remaining biases between -20% and -40% on tropospheric NO_2 VCD, especially in presence of absorbing particles and for $\tau(550\ \mathrm{nm}) \geq 0.5$. One of the main identified limitation has been the coarse sampling of the OMI cloud LUT nodes used in OMCLDO2 (see Sect. 2.2). The effect of OMCLDO2-New version on the implicit aerosol correction has not yet been analysed.

To our knowledge, no reprocessing has yet been done by applying an explicit aerosol correction based on (nearly) explicit aerosol parameters retrieved from the OMI 477 nm O_2-O_2 spectral band. Thus, the use of OMI ALH and τ parameters from Sect. 2.3 is a first attempt to apply a (nearly) explicit aerosol correction in the $A^{\mathrm{v}}_{\mathrm{NO_2}}$ computation by using visible spectral measurements from a same sensor.

DOMINO has recently evolved through the Quality Assurance for Essential Climate Variables (QA4ECV) project (www.qa4ecv.eu) which aims to address reliable and fully tracable quality information on some of the "essential climate variables" (ECVs), such as tropospheric NO_2, as defined by the Global Climate observing System (GCOS) (Lorente et al., 2017). This

reprocessing contains numerous changes in the complete chain of retrieval, from the calibrated spectrum, spectral fitting with DOAS, to the AMF computation and all the ancillary dataset. This new generation of product is expected to represent one of the best NO_2 dataset. Since the reprocessing products of QA4ECV is still under thorough validation and was not completely available at the time of this paper (and its technical work), and given our specific objective focused on the aerosol scattering and absorption correction by using information from the O_2-O_2 spectral band, the last version of DOMINO (v2) has been preferred.

The OMI cloud algorithm configuration used at the time of DOMINO-v2, and its comparison with the other algorithms are summarized in Tab. 1.

4 Results of reprocessing OMI NO_2 and $O_2 - O_2$ products

All the reprocessed OMI tropospheric NO_2 results achieved here are based on the OMI cloud and aerosol algorithms discussed in the previous sections, and summarized in Tab. 1. The main differences between the different reprocessing are synthesized in Tab. 2 for all collocated OMI-MODIS aerosol scenes.

4.1 Implicit aerosol correction - Benefits of the updated OMI cloud algorithm

Among all the main changes that are included in the updated version of OMCLDO2, the increased sampling of the OMI cloud LUT is expected to show the most important impacts on the aerosol correction (see Sect. 2.2). Indeed, the coarse sampling of the OMI cloud LUT in the former version was clearly identified by Chimot et al. (2016) as a limitation regarding the behaviour and the magnitude of c_p and thus, when deriving $N^{v}_{NO_2}$ in presence of aerosols (see Sect. 3.3). As depicted by Fig. 1, differences in c_p are now quite significant for low τ. On average, c_p from OMCLDO2-New are about 200 hPa lower than from OMCLDO2-Old (with a large standard deviation) over scenes with MODIS τ(550 nm) $\leq$ 0.5. Indeed, low aerosol load has very limited effects on $N^{s}_{O_2-O_2}$ and does not dominate the measured radiance signal. This results in large uncertainties in the retrieved c_p and a large sensitivity of the resolution at which the LUT interpolation is performed for these cases. Over scenes with high aerosol load (MODIS τ(550 nm) $\geq$ 1.0), differences are more minor and may even reverse sign. We attribute the small reverse sign to the application of the temperature correction on $N^{s}_{O_2-O_2}$ (see Sect. 2.1) which, depending on the temperature difference compared to the assumed mid-latitude summer atmosphere, may apply a positive or negative small modification of c_p in case of high τ. However, as analysed by Veefkind et al. (2016), the impact of the temperature correction on c_p remains minor in case of high c_f and thus aerosol load, compared to the updated OMI cloud LUT. Overall, all these changes are consistent with those analyzed by Veefkind et al. (2016) over cloudy scenes, with low and high c_f.

Based on synthetic cases, Figure. 2 illustrates the expected improvements of the implicit aerosol correction on $N^{v}_{NO_2}$ due to the higher OMI cloud LUT sampling. While remaining $N^{v}_{NO_2}$ biases were contained between -20 and -40 (%) with OMCLDO2-Old, they should be now limited to the range of [0:20]% with the use of OMCLDO2-New over scenes with relatively scattering or weakly absorbing aerosol particles (i.e. ω_0=0.95) and assuming a typical NO_2 summer vertical profile over north-east China. Such improvements are particularly good in case of aerosols located at an elevated altitude (i.e. more

than 1 km). However, although improved, biases can be higher in case of strongly absorbing particles: i.e. in the range of [−10:20] (%) for ω_0=0.9. Additional geophysical parameters, in particular the NO_2 profile shape, may affect these biases and are therefore of high importance (see further discussions in Sect. 5.2).

Overall, the future changes when applying the new implicit aerosol corrections from DOMINO will result from a combination of different parameters, mainly the higher sampling of the OMI cloud LUT, the temperature correction on $N^{\mathrm{s}}_{\mathrm{O_2-O_2}}$ and the updated OMI surface albedo database. To quantify the resulting changes in the reprocessed OMI $N^{\mathrm{v}}_{\mathrm{NO_2}}$, the results are separated in two categories. Firstly, Figures 3a, c and e illustrate the changes in reprocessed $N^{\mathrm{v}}_{\mathrm{NO_2}}$ from DOMINO to OMCLDO2-Old. As indicated in Tab. 1, these changes result from two consequences: 1) the temperature correction on $N^{\mathrm{s}}_{\mathrm{O_2-O_2}}$ and the new OMI surface albedo, which both directly modify the retrieval of the effective cloud parameters, and 2) the direct application of this new albedo when computing $A^{\mathrm{v}}_{\mathrm{NO_2}}$. A higher surface albedo should result in an increased length of the average light path, and therefore an enhanced $A^{\mathrm{v}}_{\mathrm{NO_2}}$. However, this can become more complex when combined with the new effective cloud parameters as they may either enhance, reduce or even counterbalance this effect. On average, $N^{\mathrm{v}}_{\mathrm{NO_2}}$ is lower (i.e. higher $A^{\mathrm{v}}_{\mathrm{NO_2}}$), between -1 $\pm$ 9 (%) in China summertime and -15.6 $\pm$ 29.8 (%) in China wintertime. The quality of these changes however depends on the accuracy of the new surface albedo climatology, which is primarily expected to be more robust due to the longer time series considered in the OMI reflectance observations (see Sect. 3.3).

Secondly, Figures 3b, d and f depict the impacts of the the implicit aerosol correction evolution from OMCLDO2-Old to OMCLDO2-New. They are directly driven by the improved c_p (see Tab. 1). Over scenes with MODIS τ(550 nm) in the range of [0.0:0.5], a decreased c_p (see Fig. 1) results in a stronger shielding (or reduced enhancement) effect from particles: $N^{\mathrm{v}}_{\mathrm{NO_2}}$ generally increases. In contrast, larger c_p over scenes with MODIS τ(550 nm) $\geq$ 1.0 leads to a lower shielding (or stronger enhancement) effect: $N^{\mathrm{v}}_{\mathrm{NO_2}}$ decreases. Standard deviation of these changes is between 15% and 20% in China wintertime and South America, and lower than 10% in China summertime and South America. Averages are in the range of [1.3:7.9]%. Regional and seasonal differences may reflect the implicit dependencies on the aerosol types, the combined effects on c_f-c_p, spatially variable surface albedo and the impacts of seasonal NO_2 vertical profile. All these observed changes are in line with the analyses deduced from the synthetic cases in Fig. 3b, d and f, confirming the improvements thanks to the updated OMI cloud LUT. Interestingly, these overall changes seem to be in line with the average AMF uncertainty of 11% evaluated by Lorente et al. (2017) due to different cloud correction scheme in polluted conditions and assuming $c_f \leq 0.2$.

Overall, maps in Fig. 4c-6c show that the total changes in $N^{\mathrm{v}}_{\mathrm{NO_2}}$, from DOMINO to OMCLDO2-New, mostly occur in the eastern part of China, where the NO_2 pollution is higher. Spatial patterns of these overall changes mostly result from a complex combination with MODIS aerosol horizontal distribution as suggested by Fig. 3, but also aerosol types, and vertical distribution: a decrease over Bejing areas in summertime, and an increase in the same area in wintertime.

4.2 Explicit aerosol correction results

In this study, there are four possibilities to apply an explicit aerosol correction from the OMI 477 nm O_2-O_2 band. Each of them differ regarding the assumed aerosol properties (i.e. ω_0), aerosol τ observations (i.e. MODIS or OMI), and the consequent

fitted ALH (see. Sect. 2.3). All these possibilities were individually applied when reprocessing the OMI DOMINO product to quantify their overall differences.

Similarly to the benefits of the new implicit aerosol correction based on OMCLDO2-New evaluated in Sect. 4.1, Fig. 7 shows the benefits of the applied explicit aerosol corrections. Provided that the aerosol model (e.g. ω_0) is in line with the actual aerosol type present in the observed scene (i.e. ideal scenario), remaining biases on $N^{\mathrm{v}}_{\mathrm{NO_2}}$ are below 20%, and little dependent on aerosol parameters (τ, ω_0 and ALH) when assuming a NO_2 vertical profile representative of a typical summer day over China east (van Noije et al., 2014; Chimot et al., 2016). In such a scenario, using either the retrieved OMI τ value or a more accurate one is not expected to make a major difference. However, in practice, these results may vary with respect to the NO_2 profile shape and additional errors in the employed aerosol model (see next subsections).

Figure 8 shows that all reprocessed $N^{\mathrm{v}}_{\mathrm{NO_2}}$ with implicit or explicit corrections are larger by [10:50]% than if no correction was performed, especially over scenes with MODIS τ(550 nm) $\geq$ 1.0. This suggests that both corrections converge to the same direction (i.e. same sign) in spite of some different magnitudes of the aerosol correction. Since all the considered strategies attenuate the $N^{\mathrm{v}}_{\mathrm{NO_2}}$ biases due to aerosols from an aerosol-free scene assumption, it is worth emphasizing that all of them, without distinction, are an aerosol correction, regardless of their implicit or (more) explicit nature.

Overall, over OMI pixels collocated with MODIS τ(550 nm) $\geq$ 0.5, Fig. 9 depicts that most of the reprocessed $N^{\mathrm{v}}_{\mathrm{NO_2}}$ values are generally higher with the explicit aerosol correction than with the implicit aerosol correction from OMCLDO2-New. This then suggests a stronger shielding effect leading to lower $A^{\mathrm{v}}_{\mathrm{NO_2}}$(439 nm). The differences increase with increasing MODIS τ as aerosol effects consequently amplify along the average light path.

In eastern China, by using the explicit aerosol correction with $NN_{MODIS,\omega_0=0.95}$, $N^{\mathrm{v}}_{\mathrm{NO_2}}$ values are higher than with the implicit aerosol correction with OMCLDO2-New by about 12 $\pm$ 12.5 % in summer and 40 $\pm$ 26.1 % in winter over scenes with MODIS τ(550 nm) $\geq$ 0.5 (see Fig. 9). The larger increase in wintertime is likely due to different NO_2 profile shapes, with NO_2 molecules being closer to the surface (see further discussions in Sect. 5.2). The differences with OMCLDO2-New are somehow reduced when assuming a lower aerosol ω_0. In such a configuration, the main differences are: 1) a lower ALH due to an assumed lower ω_0 value (Chimot et al., 2017), combined with 2) a more absorbing aerosol model used to compute $A_{\mathrm{NO_2}}$(439 nm). In both cases, $NN_{MODIS,\omega_0=0.9}$ and $NN_{MODIS,\omega_0=0.95}$, prior τ (coming from MODIS) remains unchanged. As illustrated in Figs. 9, resulting $N^{\mathrm{v}}_{\mathrm{NO_2}}$ using $NN_{MODIS,\omega_0=0.9}$ over China are smaller (i.e. $A^{\mathrm{v}}_{\mathrm{NO_2}}$(439 nm) higher) by about -0.2% $\pm$ 7.8% in summer, and -8.2% $\pm$ 22.3% in winter compared to $N^{\mathrm{v}}_{\mathrm{NO_2}}$ with $NN_{MODIS,\omega_0=0.95}$. These numbers represent then a first evaluation of the impact of aerosol model uncertainty, assuming one may use a very accurate prior τ information for both ALH retrieval and then $A^{\mathrm{v}}_{\mathrm{NO_2}}$(439 nm) computation.

Over scenes in South America with MODIS τ(550 nm) $\geq$ 0.5, the difference between $N^{\mathrm{v}}_{\mathrm{NO_2}}$ from $NN_{MODIS,\omega_0=0.95}$ and from OMCLDO2-New is on average close to zero with a standard deviation of 16.8%. The use of $NN_{MODIS,\omega_0=0.9}$ reduces $N^{\mathrm{v}}_{\mathrm{NO_2}}$ by about -1.3% $\pm$ 8.7%. Interestingly, Castellanos et al. (2015) reported an average change of 0.6% $\pm$ 8% on $A^{\mathrm{v}}_{\mathrm{NO_2}}$ after reprocessing DOMINO $N^{\mathrm{v}}_{\mathrm{NO_2}}$ over cloud-free scenes during the biomass burning season in South America and applying an explicit aerosol correction based on the OMI near-UV aerosol algorithm (OMAERUV) and CALIOP aerosol ALH.

When using the retrieved OMI τ as prior input instead of MODIS τ over eastern China, $N^{\rm v}_{\rm NO_2}$ differences with respect to the use of OMCLDO2-New differ by 5-10% on average over scenes with MODIS τ(550 nm) $\geq$ 0.6 (higher in summer but lower in winter). This suggests then a higher sensitivity to the combination of OMI τ and ALH when used together for the $A^{\rm v}_{\rm NO_2}$ computation.

Figures 4-6 show that most of the changes in $N^{\rm v}_{\rm NO_2}$ are located on the eastern part, and over areas dominated by heavy NO_2 pollutions such as the mega-cities and the Pearl River Delta. The horizontal distribution of aerosol load adds some complex patterns. Overall, the quantitative $N^{\rm v}_{\rm NO_2}$ differences between the applied explicit aerosol corrections and the improved implicit aerosol correction can be considered as an average uncertainty related to the choice of an aerosol correction approach. Similar numbers are reported by Lorente et al. (2017) who indicated an average aerosol correction uncertainty of 45% over highly polluted scenes and with large aerosol loading (τ(550 nm) $\geq$0.5). Furthermore, it was found that $N^{\rm v}_{\rm NO_2}$ from POMINO dataset over China (Lin et al., 2015) is 55% higher ($A_{\rm NO_2}$ smaller) than if no explicit aerosol correction was considered when aerosol layer is located above the tropospheric NO_2 bulk. The main identified reason was a reduced shielding effect applied by the effective cloud parameters resulting from a higher effective cloud pressure (c_p = 350 hPa): i.e. the Lambertian reflector was defined at a lower altitude. The reduction of this shielding effect may of course be attenuated when aerosols are mixed with NO_2 as their multiple scattering effects increase then the average light path length and thus the NO_2 absorption.

Finally, over scenes with little aerosol amount (i.e. MODIS τ(550 nm) $\leq$ 0.2), the difference in $N^{\rm v}_{\rm NO_2}$ between the explicit aerosol correction assuming prior MODIS τ and the implicit aerosol correction with OMCLDO2-New is systematically lower and non-null: about an average of -10% over all the considered regions. Such a difference may seem strange as so little aerosol amounts are expected to have an almost negligible effect on the light path and thus on $A^{\rm v}_{\rm NO_2}$. When OMI τ is instead considered, this difference becomes positive over China, but is reduced in absolute everywhere (less than 10%). Note that $NN_{MODIS,\omega_0=0.95}$ and $NN_{MODIS,\omega_0=0.9}$ algorithms differ from OMCLDO2 by using an external geophysical parameter (i.e. MODIS τ). Although more accurate than using the retrieved OMI τ, the combination of an external MODIS aerosol paremeter derived from different assumptions about the scattering model and surface reflectance may at the end lead to inconsistencies when combined with the OMI NN model: the 477 nm O_2-O_2 radiance budget is likely not closed. This radiance budget is always closed with OMCLDO2 (apart from the instrument noise) since it simultaneously adjusts both c_f and c_p to match with the R_c(475 nm)-$N^{\rm s}_{\rm O_2-O_2}$ combination. The topic of radiance closure budget and its impacts on $A^{\rm v}_{\rm NO_2}$ are further discussed in Sect. 5.5.

4.3 Explicit vs. implicit aerosol correction - Main reasons of the differences

As discussed in Sect. 3.2, ALH is the first crucial parameter for the computation of $A^{\rm v}_{\rm NO_2}$(439 nm). Therefore, as a first assumption, it is expected that the accuracy of the OMI ALH retrieval, and its difference with c_p, may be one of the first causes (although not unique) of the difference between the applied implicit and explicit aerosol correction.

Figure 10 compares the average OMI ALH (retrieved with the NN trained with aerosol ω_0 = 0.95) and c_p from OMCLDO2-New, both converted in metric unit (km) over cloud-free scenes and for collocated MODIS scenes with τ(550 nm) $\geq$ 0.5. Overall, both variables are quite well correlated, with similar spatial and seasonal distributions. Values are higher in China

summertime and over South America and lie in the range of [1.5:5.0] km. They are lower in China wintertime, between 0.4 and 2.0 km. Quantitatively, ALH values from $NN_{MODIS,\omega_0=0.95}$ show that the fitted aerosol layers are located higher than the fitted opaque Lambertian clouds: i.e. aerosol pressure are smaller than c_p with average differences in the range of $[-0.49{:}-50.3]$ hPa. Standard deviation of the differences are in the order of 120 hPa. The sign of the differences is reversed when employing $NN_{MODIS,\omega_0=0.9}$ (average differences 12.9-59.3 hPa).

As a first assumption, when ALH values are higher than c_p, the explicit aerosol corrections shall generally apply a stronger shielding effect on $A^{v}_{NO_2}$. Therefore, the resulting $N^{v}_{NO_2}$ should be larger. However, this only element is likely insufficient to explain the differences observed in Sect. 4.2. The combined impacts of the assumed prior τ value also play a significant rule. Furthermore, the assumed Lambertian cloud and the aerosol Henyey-Greenstein models differ about the horizontal coverage of the OMI pixel: the opaque Lambertian cloud model only covers part of the pixel (the fraction coverage is fitted through c_f, optical properties are fixed). The clear pixel fraction ensures the transmission part of the signal and the related multiple scattering not present by definition within the Lambertian cloud layer. In contrast, the aerosol model (and analysed synthetic cases) cover the whole pixels (optical properties can be changed, fraction coverage is fixed). The transmission and multiple scattering properties are included within the aerosol layer and vary as a function of the optical properties. Therefore, one can assume that in case of optically thick layers, the aerosol model generally applies a stronger screening effect by fully covering the scene and thus obstructing the surface transmission signal. By opposition, the surface transmission signal is more or less always ensured with the Lambertian opaque model by the non-covered pixel fraction.

5 Advantages and challenges of an explicit aerosol correction based on the 477 nm O_2-O_2 measurement

This section discusses specific elements in order to evaluate the relevancy of the developed explicit aerosol correction strategy over cloud-free scenes from OMI, but also in general from all UV-vis satellite measurements. In particular, we wish to draw the reader's attention to the advantage of using an explicit aerosol correction based on the exploitation of the 477 nm O_2-O_2 spectral band from a satellite measurement, but also the remaining difficulties to implement it in practice. The next subsections focus on the significance of the aerosol model error, the importance of the NO_2 vertical profile, the cases with absorbing particles, the NO_2 vertical averaging kernels, and the OMI visible radiance closure budget issue.

5.1 Impact of aerosol model error on tropospheric NO_2 air mass factor

When applying an explicit aerosol correction, the accuracy of each variable describing aerosol properties, once combined with the NO_2 vertical profile (see Sect. 5.2) and surface reflectance, overall drives the $A^{v}_{NO_2}$(439 nm) computation uncertainty. The $A^{v}_{NO_2}$ uncertainty due to this whole set of variables, not only ALH alone, can be defined as the aerosol model error for OMI $N^{v}_{NO_2}$ retrieval.

To understand, the quantitative impact of each aerosol model variable uncertainty, Figure 11 shows the $A^{v}_{NO_2}$(439 nm) biases resulting from some aerosol model inputs. A single bias on ALH of 100 hPa directly affects $N^{v}_{NO_2}$ within the range of [60:70]% when absorbing aerosols (ω_0 = 0.9) are located below 0.5 km, assuming wintertime NO_2 profile and with τ(550 nm)

= 1.4. The uncertainties are below 50% for τ(550 nm) $\leq$ 0.5, and overall below 10% when particles are located at elevated altitudes (i.e. true ALH $\geq$ 1.4 km). This quantitatively emphasizes how essential is ALH information quality when particles are actually mixed with NO_2 molecules due to the complexity to reproduce the enhancement of the average light path caused by scattering effects. A bias of 0.2 on the assumed τ(550 nm) mostly impacts scenes with little aerosol load: while resulting $N^{\mathrm{v}}_{\mathrm{NO_2}}$ uncertainties lie in the range of [$-$20:20]% for τ(550 nm) $\leq$ 0.5, they decrease to the range of [0:10]% for τ(550 nm) = 1.4. Finally, an overestimation of aerosol scattering efficiency (i.e. ω_0 bias of 0.05) leads to an underestimation of $N^{\mathrm{v}}_{\mathrm{NO_2}}$ up to -20% over scenes with high τ as a consequence of an underestimation of aerosol shielding effect and therefore a too large $A^{\mathrm{v}}_{\mathrm{NO_2}}$(439 nm). Overall, ALH uncertainty is the key driver of the AMF computation quality. ALH uncertainty must be better than 50 hPa to limit $N^{\mathrm{v}}_{\mathrm{NO_2}}$ bias below 40%. With τ uncertainty, they form the most important set of aerosol parameters prerequisite for for a high quality of $A_{\mathrm{NO_2}}$(439 nm) computation. Although not negligible, uncertainty of aerosol model parameters that are more related to the particle optical and scattering properties, such as ω_0, g and α, is of second importance provided that both ALH and τ qualities are ensured.

5.2 The importance of the relative layer height

A comprehensive aerosol correction for an accurate $A_{\mathrm{NO_2}}$(439 nm) computation also requires the actual NO_2 vertical profile. Figure 12a shows the accuracy of the aerosol corrections in $A_{\mathrm{NO_2}}$(439 nm), based on synthetic case, assuming the presence of absorbing aerosol particles (ω=0.9) but a typical NO_2 vertical profile of winter time (1st of January, 12:00 pm) over China. The main difference with Fig. 2 and Fig. 7 is the presence of a more abundant tropospheric NO_2 bulk closer to the surface, and a stronger decrease rate to higher altitudes (Chimot et al., 2016). In such a case, relative $N^{\mathrm{v}}_{\mathrm{NO_2}}$ biases with the implicit aerosol correction are strongly degraded from [$-$10:20]% (summertime) to [$-$80:40]% (winter). Already identified in Sect. 4.1 with the summer time NO_2 profile, the insufficient shielding effect applied by the effective cloud parameters from OMCLDO2-New in case of aerosol layers located in elevated altitude is here severely degraded (from -10% to -80%). The insufficient enhancement effect when particles are mixed with the tropospheric NO_2 molecules is also here amplified (from 20% to 40%).

When considering an explicit aerosol correction using $NN_{True,\omega_0=0.9}$, $N^{\mathrm{v}}_{\mathrm{NO_2}}$ bias is changed to 0-40 (%). Similarly to summertime, they are lower in case of particles at high altitude, suggesting then the strong benefits of such a correction scheme in wintertime and/or in presence of absorbing particles. The cases of aerosols close to the surface (i.e. lower than 0.5 km) remains an issue due to the difficulty to distinguish the scattering effects from the surface and the adjacent aerosol layer when retrieving ALH. The retrieval seems, in such a case, to overestimate the aerosol layer altitude.

The observed positive difference of about 40% between explicit and implicit aerosol corrections is in line with the analyses over China in wintertime (see Sect. 4.2 and Fig. 9). All these elements strongly remind and emphasize that the quality of the aerosol corrections, and their differences, for $N^{\mathrm{v}}_{\mathrm{NO_2}}$ retrieval is actually more dependent on the relative height between the particles and the tropospheric NO_2 bulk, than the absolute values of ALH or c_p themselves. The evolutions of operational aerosol correction schemes in present and future air quality UV-visible space-borne sensors, such as TROPOMI on-board Sentinel-5 Precursor, need then to consider a proper joint characterization of trace gas vertical profiles together with aerosol vertical distribution and related optical properties.

5.3 Explicit vs. implicit aerosol correction - Focus on absorbing particles

In this study, the cases with absorbing particles, i.e. aerosol ω_0 = 0.9, brings more challenges to the implicit aerosol correction than scenes dominated by more scattering aerosols. Such difficulties were also identified by Castellanos et al. (2015). For reminder, the presence of absorbing particles leads to a reduced c_p (increasing the shielding effect) but a lower c_f (lower shielding effect) with then a higher transmittance coming from the clear part of the pixel. Part of the insufficient shielding effect observed with the implicit correction in Sect. 4.1 and 5.2 may thus be explained by an insufficient coverage of the observation scene by the Lambertian opaque cloud layer: i.e. a higher fraction of the cloud-free part of the OMI scene, including the surface, is assumed leading to a higher transmittance of the associated atmospheric layers. This last element likely overall limits the potential of the effective cloud model to apply an adequate shielding effect on $A^{\mathrm{v}}_{\mathrm{NO_2}}$. However, these biases still remain lower than if no aerosol correction was achieved (Chimot et al., 2016).

Figures 7 and 12a showed the potential of the explicit aerosol correction, but by assuming no bias in the assumed τ and ω_0 parameters. To investigate further, Fig. 12c-d depict the impacts of a wrong prior aerosol ω_0 (overestimation of 0.05) when applying the explicit aerosol correction through the use of the OMI aerosol NN. When the true prior τ value for both ALH retrieval and $A^{\mathrm{v}}_{\mathrm{NO_2}}$ computation is conserved the increases of $N^{\mathrm{v}}_{\mathrm{NO_2}}$ biases are limited: from 0-40% (cf. Fig. 12a) to 0-60%. This reflects how the quality of prior τ knowledge helps to constrain both ALH retrieval, and then limit the perturbation on $A^{\mathrm{v}}_{\mathrm{NO_2}}$. However, this may be more severely degraded when inaccurate prior τ is considered (see Sect. 5.5). Figure 12d) shows the impacts of replacing true τ by the retrieved OMI one. $N^{\mathrm{v}}_{\mathrm{NO_2}}$ biases are higher, about $[-40{:}60]\%$. This is a direct result of a degradation of ALH retrieval due to a too much biased aerosol τ and the resulting impact on the $A^{\mathrm{v}}_{\mathrm{NO_2}}$. As discussed in Sect. 5.1, although ω_0 parameter is of second importance for $A^{\mathrm{v}}_{\mathrm{NO_2}}$(439 nm) itself compared to the (ALH-τ) combination, its direct impact on τ retrieval consequently affects then ALH determination accuracy and then indirectly $A^{\mathrm{v}}_{\mathrm{NO_2}}$.

In spite of these drawbacks, $N^{\mathrm{v}}_{\mathrm{NO_2}}$ biases remain smaller than if the derived effective cloud parameters are employed through the implicit aerosol correction (cf. Fig. 12a). Thus, even if imperfect, the explicit aerosol correction based on OMI ALH and τ retrievals seem to remain still advantageous for an efficient aerosol correction in tropospheric NO_2 VCD retrieval from visible satellite radiance. Nevertheless, true horizontal distributions of aerosols within the observation pixel may actually be quite heterogeneous. Such problems should be further investigated with a focus on areas where absorbing particles are expected such as in winter time in China, or during large biomass burning episodes. Future studies should also determine how often such effect occurs and its overall impact depending on the NO_2 vertical profile variability.

5.4 Aerosol model and NO_2 vertical averaging kernel

Theoretically, the application of an explicit aerosol model is expected to simulate more realistic scattering and absorption effects due to particles when computing $A_{\mathrm{NO_2}}$(439 nm). Figure 13 illustrates the vertical averaging kernel (AK) (cf. Sect. 3.2) assuming τ(550 nm) = 1.0 and from the application of OMCLDO2-New, $NN_{MODIS,\omega_0=0.95}$ and true aerosol conditions, assuming no bias in prior aerosol assumptions. AKs are very important for estimating the surface NO_x emissions by convoluting the NO_2 vertical profiles from the used atmospheric models to match with the OMI $N^{\mathrm{v}}_{\mathrm{NO_2}}$ observations (Eskes and Boersma,

2003; Ding et al., 2015). AKs based on OMCLDO2-New display a sharp distinction between the enhanced atmospheric layers located above aerosols and the shielded layers located below. On the contrary, AKs from $NN_{MODIS,\omega_0=0.95}$ depict a smoother transition from then enhanced to the shielded layers. This transition is more in line with the actual AKs (Fig. 13a) and results from the scattering effects induced by the more or less wide aerosol particle layer. A bright Lambertian reflector is by nature fully opaque and does not induce multiple scattering effects. This is partly compensated by the transmission of the clear fraction of the pixel through the IPA assumption (see Sect. 2.2). This suggests that applying an explicit aerosol correction leads to the consideration of more realistic physical assumptions and AK productions. However, such a suggestion critically depends on an ensemble of other parameters that contribute to the AK generation: the accuracy of the retrieved ALH which triggers the location of the enhancement / shielding transition, the potential aerosol model biases (e.g. ω_0, scattering phase function, etc...), and the difference between actual and assumed aerosol vertical profile.

5.5 Radiance closure budget issue and potential impacts

The discussions about the "model error" in the previous sub-sections implicitly made the assumption that the whole set of parameters such as (c_f-c_p-surface reflectance) on the one hand, or (τ-ALH-ω_o-g-α-surface reflectance) are fully consistent in the sense that they form one unique particle model. However, when external data are used to constrain ALH retrieval accuracy, such as MODIS aerosol τ, one may combine inconsistent model assumptions together leading then to complex artefacts such as the issue of OMI closure radiance budget.

Radiance closure budget is not only important in the 477 nm O_2-O_2 band, but also in the NO_2 absorption band at the wavelength where the AMF is computed. Aerosol τ combined with surface reflectance are expected to drive OMI R_c(475 nm). As discussed in Sect. 2.2, OMCLDO2 simultaneously adjusts both c_f and c_p based on the same prior surface reflectance such that their combination allows to close the (R_c(475 nm)-$N^{\mathrm{s}}_{\mathrm{O_2}-O_2}$) budget, and thus the OMI 477 nm O_2-O_2 radiance regardless the accuracy of the selected model. On the contrary, by using MODIS τ, only OMI $N^{\mathrm{s}}_{\mathrm{O_2}-O_2}$ is exploited, not R_c(475 nm). If all the prior parameters are accurate and derived from a unique set of aerosol model and surface reflectance parameters, the (R_c(475 nm)-$N^{\mathrm{s}}_{\mathrm{O_2}-O_2}$) budget should be closed. However, any mismatch between the model employed for MODIS τ determination and the one used in the OMI NN training dataset, between MODIS and OMI instrument radiance, and/ or the surface reflectance hypothesis may leave this budget open. In particularly, it is worth reminding that the surface reflectance dataset behind MODIS τ, OMI c_f and $A^{\mathrm{v}}_{\mathrm{NO_2}}$(439 nm) are not identical: for OMI , a multi-spectral surface Lambertian equivalent reflectance (LER) was used(Kleipool et al., 2008) while MODIS aerosol retrieval uses a directional surface spectral reflectance (Levy et al., 2013).

Therefore, the strategies of implicit vs. explicit aerosol correction analysed in Sect. 4.2 do not only differ in terms of assumed particle optical and scattering property model but also on how much the whole OMI radiance budget is eventually fitted. This last difference likely explains the strange systematic difference (about -10%) identified over OMI scenes with MODIS τ(550 nm) ≤ 0.2, where aerosol effects could be assumed as almost insignificant (see Fig. 9). When. MODIS τ is replaced by the retrieved OMI τ (see. Tab. 1) which is, like c_f, mostly constrained by R_c(475 nm), prior OMI surface albedo and the same aerosol model used for ALH retrieval and $A^{\mathrm{v}}_{\mathrm{NO_2}}$(439 nm) calculation, resulting $N^{\mathrm{v}}_{\mathrm{NO_2}}$ are higher than with the use of MODIS

τ (see Tab. 2). Moreover, as analysed in Sect. 4.2, the differences between the implicit and explicit aerosol corrections are in absolute smaller everywhere over scenes with small aerosol load confirming the consistency in the employed models for each set of parameters and an almost complete closure of the OMI visible radiance budget (instrument noise apart).

At the end, one might wonder what the best option is for an optimal aerosol correction: 1) using the best aerosol and surface parameters available for the most accurate correction at the cost of not closing the satellite radiance budget, or 2) applying a less accurate correction but with an ensemble of aerosol and surface parameters that eventually comprehensively fit the spectral measurement. The first option gives more weights to the used auxiliary data, while the second option maximises the weights of the amount of information contained in the satellite measurement. The answer to such a problem is, in our opinion, not clear at this moment. But, given the fact that several studies prioritise the application of multiple parameters from very diverse sources (models, ancillary instruments with different techniques, etc..) to satellite spectral measurements, we think that the issue of radiance closure budget should be kept in mind by the scientific community and further investigated in future research studies. At the end, an optimal trade off must be found between quality of $N^{\mathrm{v}}_{\mathrm{NO_2}}$ product and the weights given to the original satellite measurement.

6 Conclusions

This paper reprocesses of the reference OMI tropospheric NO_2 vertical column density $N^{\mathrm{v}}_{\mathrm{NO_2}}$ for cloud-free scenes over east China and South America for 2006 and 2007. These regions are dominated by high aerosol loadings. The goal of this study is to evaluate the benefits of the recent achieved developments during the last years to improve the so-called aerosol correction in the tropospheric NO_2 air mass factor $A^{\mathrm{v}}_{\mathrm{NO_2}}$, a crucial parameter when retrieving $N^{\mathrm{v}}_{\mathrm{NO_2}}$ from visible air quality satellite backscattered measurements. In particular, the tested aerosol correction strategies rely on our recent experiences with the 477 nm O_2-O_2 spectral band: a key spectral band present in current and future air quality UV-vis satellite instruments such as OMI, GOME-2, TROPOMI, Sentinel-4-UVN, and Sentinel-5-UVNS. The use of this band is important in view of operational data processing as it allows to derive parameters that, in principle, could reproduce the particle scattering and absorption effects on the average light path in the visible spectral window and representative of the sensor field of view. Regardless of the type of algorithm employed here, these parameters can all be derived using computationally inexpensive methods, are directly representative of the OMI pixel in terms of spectral measurement, spatial coverage and temporal acquisition, and can directly be used for the $A^{\mathrm{v}}_{\mathrm{NO_2}}$ computation.

The two tested algorithms are the OMI cloud software OMCLDO2 (Veefkind et al., 2016), and the OMI aerosol Neural Network (NN) approach (Chimot et al., 2017, 2018). The most important difference between these methods is the assumed aerosol model, not only for the retrieval of the aerosol parameters in the O_2-O_2 band, but also how they represent the aerosol effect in the tropospheric NO_2 air mass factor. The OMCLDO2 represents the aerosols as effective cloud parameters and thus implicitly correct the aerosol effects, whereas the NN approach explicitly models and corrects for aerosols. The most recent OMCLDO2 update from (Veefkind et al., 2016) includes, among many elements, an increased number of nodes in the lookup-tables and the necessary temperature correction on the O_2-O_2 slant column density.

For both methods, the reprocessed $N^{\mathrm{v}}_{\mathrm{NO_2}}$ shows smaller biases over cloud-free scenes dominated by aerosol pollution, compared to the standard DOMINO retrieval and its related aerosol correction. Previous studies showed an underestimation of the OMI $N^{\mathrm{v}}_{\mathrm{NO_2}}$ between -20% and -40% over scenes with MODIS aerosol optical thickness $\tau(550\,\mathrm{nm}) \geq 0.6$, assuming scattering aerosol particles with aerosol single scattering albedo $\omega_0 = 0.95$ and summertime NO_2 vertical profile. In similar conditions, these biases are expected to be contained in the limit of [0:20]%, for both the most recent OMCLDO2 method and the NN method. On average, the applied explicit NN correction leads to higher $N^{\mathrm{v}}_{\mathrm{NO_2}}$ values compared to the implicit OMCLDO2 correction up to 40% depending on the seasons, regions and aerosol pollution episodes. This represents our best estimate of the aerosol correction uncertainty for the OMI $N^{\mathrm{v}}_{\mathrm{NO_2}}$ retrieval due to the possible choices of the algorithm correction. They are attributed to the model differences and the associated output variables.

Although both the implicit OMCLDO2 and explicit NN methods are a significant improvement over the current OMI DOMINO retrieval, we also found limitations that need to be further studied:

- If absorbing aerosols (i.e. single scattering albedo $\omega_0 \leq 0.9$) are present, the implicit aerosol correction still leads to substantial biases on $N^{\mathrm{v}}_{\mathrm{NO_2}}$ due to an insufficient applied shielding effect: between -80% and 20% assuming a typical NO_2 wintertime profile . This is most severe when particles are located at high altitude (above 1.4 km) and with heavy aerosol load. In similar conditions, the explicit aerosol correction allows to mitigate the biases to the range of [0:40]% if accurate τ and aerosol model are available, or $[-40{:}60]\%$ with inaccurate τ (e.g. retrieved OMI τ) and aerosol model.

- Biases remain high when particles are located close to the surface, regardless of the aerosol correction methodology. The distinction between aerosol scattering and surface reflectance is challenging under such conditions. Since particles are close to the tropospheric NO_2 bulk (either mixed or slightly above), small errors in the retrieved aerosol height or effective cloud pressure have a significant impact on the derived NO_2 column.

- All aerosol correction methodologies are sensitive to the NO_2 vertical profile and the employed surface albedo or reflectance. Future improvements need to address both these parameters together with any evolution that can still be done in the aerosol or effective cloud retrievals from the 477 nm O_2-O_2.

- Although the OMI aerosol NN algorithms lead to promising ALH retrieval, its use for an explicit aerosol correction is not straightforward. Indeed, ALH is only one variable (although a key one) of a set of aerosol parameters that need to be applied for the required explicit aerosol correction. Its combination with other aerosol parameters (size, ω_0, τ) can lead either to model errors and/or to the risk of not closing the OMI radiance budget if any of these parameters was issued from an external source (model or instrument) not consistent with the OMI ALH retrieval.

Based on its estimated performances, we recommend for an operational processing of OMI data, where no distinction is made between cloudy, cloud-free, and aerosol contaminated scenes, to use firstly the implicit aerosol correction based on OMCLDO2. It allows to correct adequately both cloud and aerosol particle effects on the average light path. If, cloud-free scenes can be carefully identified and collected in a same way it has been done here, then the explicit aerosol correction based on the OMI

NN aerosol algorithms should be considered. We demonstrated in this study, for the first time, its high performance and the realism of the simulated physical effects. Moreover, the developed NN approach can ensure a fast cloud-free data processing.

Overall, the considered aerosol corrections can in principle be transposed to the future generation of air quality UV-vis satellite sensors, such as TROPOMI, Sentinel-4, and Sentinel-5-UVNS. It can also be considered for other trace gases of interest: e.g. O_2, HCHO. However, such an approach has to be adapted to the specificities of this new generation of instruments.

Code and data availability. All the data results and specific algorithms created in this study are available from the authors upon request. If you are interested to have access to them, please send a message to Julien.Chimot@eumetsat.int and pepijn.veefkind@knmi.nl. The pybrain library code is available at http://pybrain.org/. Finally, The OMCLDO2 dataset is available from the NASA archives: https://disc.gsfc.nasa.gov/uui/datasets/OMCLDO2_003/summary.

Competing interests. The authors declare that they have no conflict of interest.

Acknowledgements. This work was funded by the Netherlands Space Office (NSO) under the OMI contract.The authors thank Johanna Tamminen from the Finnish Meteorological Institue (FMI), Thomas Wagner from Max Plank Institute (MPI), Ilse Aben from SRON Netherlands Institute for Space Research and Folkert Boersma from KNMI for the reviews and discussions.

References

Acarreta, J. R., de Haan, J. F., and Stammes, P.: Cloud pressure retrieval using the O_2-O_2 absorption band at 477 nm, Journal of Geophysical Research: Atmospheres, 109, n/a–n/a, https://doi.org/10.1029/2003JD003915, http://dx.doi.org/10.1029/2003JD003915, d05204, 2004.

Amiridis, V., Marinou, E., Tsekeri, A., Wandinger, U., Schwarz, A., Giannakaki, E., Mamouri, R., Kokkalis, P., Binietoglou, I., Solomos, S., Herekakis, T., Kazadzis, S., Gerasopoulos, E., Proestakis, E., Kottas, M., Balis, D., Papayannis, A., Kontoes, C., Kourtidis, K., Papagiannopoulos, N., Mona, L., Pappalardo, G., Le Rille, O., and Ansmann, A.: LIVAS: a 3-D multi-wavelength aerosol/cloud database based on CALIPSO and EARLINET, Atmospheric Chemistry and Physics, 15, 7127–7153, https://doi.org/10.5194/acp-15-7127-2015, http://www.atmos-chem-phys.net/15/7127/2015/, 2015.

Boersma, K. F., Eskes, H. J., and Brinksma, E. J.: Error analysis for tropospheric NO2 retrieval from space, Journal of Geophysical Research: Atmospheres, 109, n/a–n/a, https://doi.org/10.1029/2003JD003962, http://dx.doi.org/10.1029/2003JD003962, d04311, 2004.

Boersma, K. F., Eskes, H. J., Veefkind, J. P., Brinksma, E. J., van der A, R. J., Sneep, M., van den Oord, G. H. J., Levelt, P. F., Stammes, P., Gleason, J. F., and Bucsela, E. J.: Near-real time retrieval of tropospheric NO_2 from OMI, Atmospheric Chemistry and Physics, 7, 2103–2118, https://doi.org/10.5194/acp-7-2103-2007, http://www.atmos-chem-phys.net/7/2103/2007/, 2007.

Boersma, K. F., Eskes, H. J., Dirksen, R. J., van der A, R. J., Veefkind, J. P., Stammes, P., Huijnen, V., Kleipool, Q. L., Sneep, M., Claas, J., Leitao, J., Richter, A., Zhou, Y., and Brunner, D.: An improved tropospheric NO_2 column retrieval algorithm for the Ozone Monitoring Instrument, Atmospheric Measurement Techniques, 4, 1905–1928, https://doi.org/10.5194/amt-4-1905-2011, http://www.atmos-meas-tech.net/4/1905/2011/, 2011.

Bousserez, N.: Space-based retrieval of NO_2 over biomass burning regions: quantifying and reducing uncertainties, Atmospheric Measurement Techniques, 7, 3431–3444, https://doi.org/10.5194/amt-7-3431-2014, https://www.atmos-meas-tech.net/7/3431/2014/, 2014.

Castellanos, P., Boersma, K. F., Torres, O., and de Haan, J. F.: OMI tropospheric NO_2 air mass factors over South America: effects of biomass burning aerosols, Atmospheric Measurement Techniques, 8, 3831–3849, https://doi.org/10.5194/amt-8-3831-2015, http://www.atmos-meas-tech.net/8/3831/2015/, 2015.

Chimot, J., Vlemmix, T., Veefkind, J. P., de Haan, J. F., and Levelt, P. F.: Impact of aerosols on the OMI tropospheric NO_2 retrievals over industrialized regions: how accurate is the aerosol correction of cloud-free scenes via a simple cloud model?, Atmospheric Measurement Techniques, 9, 359–382, https://doi.org/10.5194/amt-9-359-2016, http://www.atmos-meas-tech.net/9/359/2016/, 2016.

Chimot, J., Veefkind, J. P., Vlemmix, T., de Haan, J. F., Amiridis, V., Proestakis, E., Marinou, E., and Levelt, P. F.: An exploratory study on the aerosol height retrieval from OMI measurements of the 477 nm O_2-O_2 spectral band using a neural network approach, Atmospheric Measurement Techniques, 10, 783–809, https://doi.org/10.5194/amt-10-783-2017, http://www.atmos-meas-tech.net/10/783/2017/, 2017.

Chimot, J., Veefkind, J. P., Vlemmix, T., and Levelt, P. F.: Spatial distribution analysis of the OMI aerosol layer height: a pixel-by-pixel comparison to CALIOP observations, Atmospheric Measurement Techniques, 11, 2257–2277, https://doi.org/10.5194/amt-11-2257-2018, https://www.atmos-meas-tech.net/11/2257/2018/, 2018.

Colosimo, S. F., Natraj, V., Sander, S. P., and Stutz, J.: A sensitivity study on the retrieval of aerosol vertical profiles using the oxygen A-band, Atmospheric Measurement Techniques, 9, 1889–1905, https://doi.org/10.5194/amt-9-1889-2016, http://www.atmos-meas-tech.net/9/1889/2016/, 2016.

Curier, R., Kranenburg, R., Segers, A., Timmermans, R., and Schaap, M.: Synergistic use of OMI NO_2 tropospheric columns and LOTOS–EUROS to evaluate the NO_x emission trends across Europe, Remote Sensing of Environment, 149, 58 – 69, https://doi.org/https://doi.org/10.1016/j.rse.2014.03.032, http://www.sciencedirect.com/science/article/pii/S0034425714001321, 2014.

de Haan, J. F.: DISAMAR Algorithm Description and Background Information, Royal Netherlands Meteorological Institute, De Bilt, the Netherlands, 2011.

De Smedt, I., Theys, N., Yu, H., Danckaert, T., Lerot, C., Compernolle, S., Van Roozendael, M., Richter, A., Hilboll, A., Peters, E., Pedergnana, M., Loyola, D., Beirle, S., Wagner, T., Eskes, H., van Geffen, J., Boersma, K. F., and Veefkind, P.: Algorithm Theoretical Baseline for formaldehyde retrievals from S5P TROPOMI and from the QA4ECV project, Atmospheric Measurement Techniques Discussions, 2017, 1–53, https://doi.org/10.5194/amt-2017-393, https://www.atmos-meas-tech-discuss.net/amt-2017-393/, 2017.

Ding, J., van der A, R. J., Mijling, B., Levelt, P. F., and Hao, N.: NO_x emission estimates during the 2014 Youth Olympic Games in Nanjing, Atmospheric Chemistry and Physics, 15, 9399–9412, https://doi.org/10.5194/acp-15-9399-2015, https://www.atmos-chem-phys.net/15/9399/2015/, 2015.

Dubovik, O., Holben, B., Eck, T. F., Smirnov, A., Kaufman, Y. J., King, M. D., Tanré, D., and Slutsker, I.: Variability of Absorption and Optical Properties of Key Aerosol Types Observed in Worldwide Locations, Journal of the Atmospheric Sciences, 59, 590–608, https://doi.org/10.1175/1520-0469(2002)059<0590:VOAAOP>2.0.CO;2, http://dx.doi.org/10.1175/1520-0469(2002)059<0590:VOAAOP>2.0.CO;2, 2002.

Duncan, B., Lamsal, L., Thompson, A., Yoshida, Y., Lu, Z., Streets, D., Hurwitz, M., and Pickering, K.: A space-based, high-resolution view of notable changes in urban NO_x pollution around the world (2005–2014), Journal of Geophysical Research: Atmospheres, 121, 976–996, https://doi.org/10.1002/2015JD024121, http://dx.doi.org/10.1002/2015JD024121, 2015JD024121, 2016.

Eskes, H. and Boersma, K.: Averaging kernels for DOAS total-column satellite retrievals, Atmospheric Chemistry and Physics, 3, 1285–1291, https://doi.org/10.5194/acp-3-1285-2003, https://www.atmos-chem-phys.net/3/1285/2003/, 2003.

Hovenier, J. W. and Hage, J. I.: Relations involving the spherical albedo and other photometric quantities of planets with thick atmospheres, Astron. Astrophys., 214, 391–401, http://adsabs.harvard.edu/abs/1989A%26A...214..391H, provided by the SAO/NASA Astrophysics Data System, 1989.

Ingmann, I., Veihelmann, B., Langen, J., Lamarre, D., Stark, H., and Bazalgette Courrèges-Lacoste, G.: Requirements for the GMES Atmosphere Service and ESA's implementation concept: Sentinels-4/-5 and -5p, Remote Sensing of Environment, 120, 58 – 69, https://doi.org/https://doi.org/10.1016/j.rse.2012.01.023, http://www.sciencedirect.com/science/article/pii/S0034425712000673, the Sentinel Missions - New Opportunities for Science, 2012.

Joiner, J., Vasilkov, A. P., Flittner, D. E., Gleason, J. F., and Bhartia, P. K.: Retrieval of cloud pressure and oceanic chlorophyll content using Raman scattering in GOME ultraviolet spectra, Journal of Geophysical Research: Atmospheres, 109, https://doi.org/10.1029/2003JD003698, https://agupubs.onlinelibrary.wiley.com/doi/abs/10.1029/2003JD003698, 2004.

Kleipool, Q. L., Dobber, M. R., de Haan, J. F., and Levelt, P. F.: Earth surface reflectance climatology from 3 years of OMI data, Journal of Geophysical Research: Atmospheres, 113, n/a–n/a, https://doi.org/10.1029/2008JD010290, http://dx.doi.org/10.1029/2008JD010290, d18308, 2008.

Leitão, J., Richter, A., Vrekoussis, M., Kokhanovsky, A., Zhang, Q. J., Beekmann, M., and Burrows, J. P.: On the improvement of NO_2 satellite retrievals – aerosol impact on the airmass factors, Atmospheric Measurement Techniques, 3, 475–493, https://doi.org/10.5194/amt-3-475-2010, http://www.atmos-meas-tech.net/3/475/2010/, 2010.

Levy, R. C., Mattoo, S., Munchak, L. A., Remer, L. A., Sayer, A. M., Patadia, F., and Hsu, N. C.: The Collection 6 MODIS aerosol products over land and ocean, Atmospheric Measurement Techniques, 6, 2989–3034, https://doi.org/10.5194/amt-6-2989-2013, http://www.atmos-meas-tech.net/6/2989/2013/, 2013.

Lin, J.-T., Martin, R. V., Boersma, K. F., Sneep, M., Stammes, P., Spurr, R., Wang, P., Van Roozendael, M., Clémer, K., and Irie, H.: Retrieving tropospheric nitrogen dioxide from the Ozone Monitoring Instrument: effects of aerosols, surface reflectance anisotropy, and vertical profile of nitrogen dioxide, Atmospheric Chemistry and Physics, 14, 1441–1461, https://doi.org/10.5194/acp-14-1441-2014, http://www.atmos-chem-phys.net/14/1441/2014/, 2014.

Lin, J.-T., Liu, M.-Y., Xin, J.-Y., Boersma, K. F., Spurr, R., Martin, R., and Zhang, Q.: Influence of aerosols and surface reflectance on satellite NO_2 retrieval: seasonal and spatial characteristics and implications for NO_x emission constraints, Atmospheric Chemistry and Physics, 15, 11 217–11 241, https://doi.org/10.5194/acp-15-11217-2015, http://www.atmos-chem-phys.net/15/11217/2015/, 2015.

Liu, M., Lin, J., Boersma, K. F., Pinardi, G., Wang, Y., Chimot, J., Wagner, T., Xie, P., Eskes, H., Van Roozendael, M., Hendrick, F., Wang, P., and Yan, Y.: Improved aerosol correction for OMI tropospheric NO_2 retrieval over East Asia: constraint from CALIOP aerosol vertical profile, Atmospheric Measurement Techniques Discussions, 2018, 1–48, https://doi.org/10.5194/amt-2018-34, https://www.atmos-meas-tech-discuss.net/amt-2018-34/, 2018.

Lorente, A., Folkert Boersma, K., Yu, H., Dörner, S., Hilboll, A., Richter, A., Liu, M., Lamsal, L. N., Barkley, M., De Smedt, I., Van Roozendael, M., Wang, Y., Wagner, T., Beirle, S., Lin, J.-T., Krotkov, N., Stammes, P., Wang, P., Eskes, H. J., and Krol, M.: Structural uncertainty in air mass factor calculation for NO_2 and HCHO satellite retrievals, Atmospheric Measurement Techniques, 10, 759–782, https://doi.org/10.5194/amt-10-759-2017, https://www.atmos-meas-tech.net/10/759/2017/, 2017.

Martin, R., Chance, K., Jacob, D., Kurosu, T., Spurr, R., Bucsela, E., Gleason, J., Palmer, P., Bey, I., Fiore, A., Li, Q., Yantosca, R., and Koelemeijer, R.: An improved retrieval of tropospheric nitrogen dioxide from GOME, Journal of Geophysical Research: Atmospheres, 107, ACH 9–1–ACH 9–21, https://doi.org/10.1029/2001JD001027, http://dx.doi.org/10.1029/2001JD001027, 4437, 2002.

Martin, R., Jacob, D., Chance, K., Kurosu, T., Palmer, P., and Evans, M.: Global inventory of nitrogen oxide emissions constrained by space-based observations of NO_2 columns, Journal of Geophysical Research: Atmospheres, 108, n/a–n/a, https://doi.org/10.1029/2003JD003453, http://dx.doi.org/10.1029/2003JD003453, 4537, 2003.

Nanda, S., de Graaf, M., Sneep, M., de Haan, J. F., Stammes, P., Sanders, A. F. J., Tuinder, O., Veefkind, J. P., and Levelt, P. F.: Error sources in the retrieval of aerosol information over bright surfaces from satellite measurements in the oxygen A-band, Atmospheric Measurement Techniques Discussions, 2017, 1–26, https://doi.org/10.5194/amt-2017-323, https://www.atmos-meas-tech-discuss.net/amt-2017-323/, 2017.

Palmer, P., Jacob, D., Chance, K., Martin, R., Spurr, R., Kurosu, T., Bey, I., Yantosca, R., Fiore, A., and Li, Q.: Air mass factor formulation for spectroscopic measurements from satellites: Application to formaldehyde retrievals from the Global Ozone Monitoring Experiment, Journal of Geophysical Research: Atmospheres, 106, 14 539–14 550, https://doi.org/10.1029/2000JD900772, http://dx.doi.org/10.1029/2000JD900772, 2001.

Park, S. S., Kim, J., Lee, H., Torres, O., Lee, K.-M., and Lee, S. D.: Utilization of O_4 slant column density to derive aerosol layer height from a space-borne UV–visible hyperspectral sensor: sensitivity and case study, Atmospheric Chemistry and Physics, 16, 1987–2006, https://doi.org/10.5194/acp-16-1987-2016, http://www.atmos-chem-phys.net/16/1987/2016/, 2016.

Platt, U. and Stutz, J.: Differential Optical Absorption Spectroscopy (DOAS), Principles and Applications, Springer-Verlag Berlin Heidelberg, https://doi.org/10.1007/978-3-540-75776-4, 2008.

Reuter, M., Buchwitz, M., Hilboll, A., Richter, A., Schneising, O., Hilker, M., Heymann, J., Bovensmann, H., and Burrows, J. P.: Decreasing emissions of NO_x relative to CO_2 in East Asia inferred from satellite observations, Nat. Geosci. Lett., 7, 792–795, https://doi.org/10.1038/NGEO2257, 2014.

Richter, A. and Burrows, J.: Tropospheric NO_2 from GOME measurements, Advances in Space Research, 29, 1673–1683, https://doi.org/https://doi.org/10.1016/S0273-1177(02)00100-X, http://www.sciencedirect.com/science/article/pii/S027311770200100X, 2002.

Richter, A. and Wagner, T.: The Use of UV in Visible and Near IR Solar Back Scattered Radiation to Determine Trace Gases, The Remote Sensingof Tropospheric Composition from Space, Physics of Earth and Space Environments, Chapter 2, Springer-Verlag Berlin Heidelberg,, 10.1007/978-3-642-14791-3, 2011.

Rozanov, V. V. and Rozanov, A. V.: Differential optical absorption spectroscopy (DOAS) and air mass factor concept for a multiply scattering vertically inhomogeneous medium: theoretical consideration, Atmospheric Measurement Techniques, 3, 751–780, https://doi.org/10.5194/amt-3-751-2010, https://www.atmos-meas-tech.net/3/751/2010/, 2010.

Sanders, A. F. J., de Haan, J. F., Sneep, M., Apituley, A., Stammes, P., Vieitez, M. O., Tilstra, L. G., Tuinder, O. N. E., Koning, C. E., and Veefkind, J. P.: Evaluation of the operational Aerosol Layer Height retrieval algorithm for Sentinel-5 Precursor: application to O_2 A band observations from GOME-2A, Atmospheric Measurement Techniques, 8, 4947–4977, https://doi.org/10.5194/amt-8-4947-2015, http://www.atmos-meas-tech.net/8/4947/2015/, 2015.

Sneep, M., de Haan, J. F., Stammes, P., Wang, P., Vanbauce, C., Joiner, J., Vasilkov, A. P., and Levelt, P. F.: Three-way comparison between OMI and PARASOL cloud pressure products, Journal of Geophysical Research: Atmospheres, 113, n/a–n/a, https://doi.org/10.1029/2007JD008694, http://dx.doi.org/10.1029/2007JD008694, d15S23, 2008.

Spada, F., Krol, M. C., and Stammes, P.: McSCIA: application of the Equivalence Theorem in a Monte Carlo radiative transfer model for spherical shell atmospheres, Atmospheric Chemistry and Physics, 6, 4823–4842, https://doi.org/10.5194/acp-6-4823-2006, http://www.atmos-chem-phys.net/6/4823/2006/, 2006.

Stammes, P., Sneep, M., de Haan, J., Veefkind, J., Wang, P., and Levelt, P.: Effective cloud fractions from the Ozone Monitoring Instrument: Theoretical framework and validation, Journal of Geophysical Research: Atmospheres, 113, n/a–n/a, https://doi.org/10.1029/2007JD008820, http://dx.doi.org/10.1029/2007JD008820, d16S38, 2008.

van Noije, T., Le Sager, P., Segers, A., van Velthoven, P., Krol, M., Hazeleger, W., Williams, A., and Chambers, S.: Simulation of tropospheric chemistry and aerosols with the climate model EC-Earth, Geoscientific Model Development, 7, 2435–2475, https://doi.org/10.5194/gmd-7-2435-2014, https://www.geosci-model-dev.net/7/2435/2014/, 2014.

Vasilkov, A., Yang, E.-S., Marchenko, S., Qin, W., Lamsal, L., Joiner, J., Krotkov, N., Haffner, D., Bhartia, P. K., and Spurr, R.: A cloud algorithm based on the O_2-O_2 477 nm absorption band featuring an advanced spectral fitting method and the use of surface geometry-dependent Lambertian-equivalent reflectivity, Atmospheric Measurement Techniques, 11, 4093–4107, https://doi.org/10.5194/amt-11-4093-2018, https://www.atmos-meas-tech.net/11/4093/2018/, 2018.

Veefkind, J. P., Boersma, K. F., Wang, J., Kurosu, T. P., Krotkov, N., Chance, K., and Levelt, P. F.: Global satellite analysis of the relation between aerosols and short-lived trace gases, Atmospheric Chemistry and Physics, 11, 1255–1267, https://doi.org/10.5194/acp-11-1255-2011, http://www.atmos-chem-phys.net/11/1255/2011/, 2011.

Veefkind, J. P., Aben, I., McMullan, K., Förster, H., de Vries, J., Otter, G., Claas, J., Eskes, H. J., de Haan, J. F., Kleipool, Q., van Weele, M., Hasekamp, O., Hoogeveen, R., Landgraf, J., Snel, R., Tol, P., Ingmann, P., Voors, R., Kruizinga, B., Vink, R., Visser, H., and Levelt, P. F.: TROPOMI on the ESA Sentinel-5 Precursor: A GMES mission for global observations of the atmospheric composition for climate, air quality and ozone layer applications, Remote sensing of environment., 120, 70—83, https://doi.org/10.1016/j.rse.2011.09.027, http://dx.doi.org/10.1016/j.rse.2011.09.027, 2012.

Veefkind, J. P., de Haan, J. F., Sneep, M., and Levelt, P. F.: Improvements of the OMI O_2-O_2 Operational Cloud Algorithm and Comparisons with Ground-Based Radar-Lidar Observations, Atmospheric Measurement Techniques Discussions, 2016, 1–28, https://doi.org/10.5194/amt-2016-48, http://www.atmos-meas-tech-discuss.net/amt-2016-48/, 2016.

Vlemmix, T., Piters, A. J. M., Stammes, P., Wang, P., and Levelt, P. F.: Retrieval of tropospheric NO_2 using the MAX-DOAS method combined with relative intensity measurements for aerosol correction, Atmospheric Measurement Techniques, 3, 1287–1305, https://doi.org/10.5194/amt-3-1287-2010, http://www.atmos-meas-tech.net/3/1287/2010/, 2010.

Wagner, T., Dix, B., Friedeburg, C. v., Frieß, U., Sanghavi, S., Sinreich, R., and Platt, U.: MAX-DOAS O_4 measurements: A new technique to derive information on atmospheric aerosols—Principles and information content, Journal of Geophysical Research: Atmospheres, 109, n/a–n/a, https://doi.org/10.1029/2004JD004904, http://dx.doi.org/10.1029/2004JD004904, d22205, 2004.

Wagner, T., Burrows, J. P., Deutschmann, T., Dix, B., von Friedeburg, C., Frieß, U., Hendrick, F., Heue, K.-P., Irie, H., Iwabuchi, H., Kanaya, Y., Keller, J., McLinden, C. A., Oetjen, H., Palazzi, E., Petritoli, A., Platt, U., Postylyakov, O., Pukite, J., Richter, A., van Roozendael, M., Rozanov, A., Rozanov, V., Sinreich, R., Sanghavi, S., and Wittrock, F.: Comparison of box-air-mass-factors and radiances for Multiple-Axis Differential Optical Absorption Spectroscopy (MAX-DOAS) geometries calculated from different UV/visible radiative transfer models, Atmospheric Chemistry and Physics, 7, 1809–1833, https://doi.org/10.5194/acp-7-1809-2007, http://www.atmos-chem-phys.net/7/1809/2007/, 2007.

Wang, Y., Penning de Vries, M., Xie, P. H., Beirle, S., Dörner, S., Remmers, J., Li, A., and Wagner, T.: Cloud and aerosol classification for 2.5 years of MAX-DOAS observations in Wuxi (China) and comparison to independent data sets, Atmospheric Measurement Techniques, 8, 5133–5156, https://doi.org/10.5194/amt-8-5133-2015, https://www.atmos-meas-tech.net/8/5133/2015/, 2015.

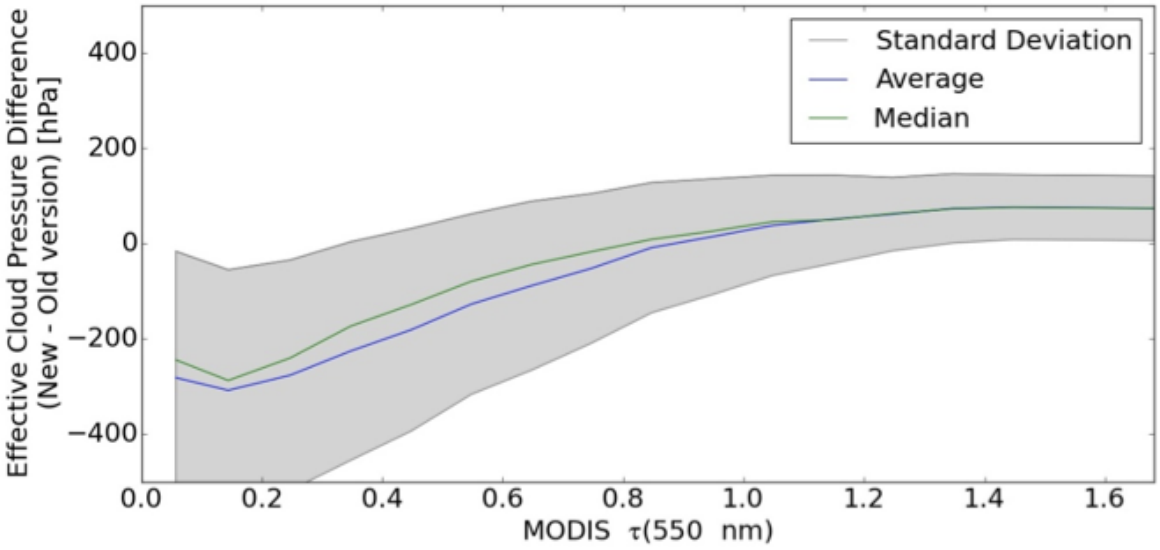

Figure 1. Statistics of effective cloud pressure differences between OMCLDO2-new and OMCLDO2-old (see Sect. 2.2 and Tab. 1) in [hPa] in 2006-2007 as a function of MODIS aerosol optical thickness (AOT) τ(550 nm). An example over China in summertime (June-July-August).

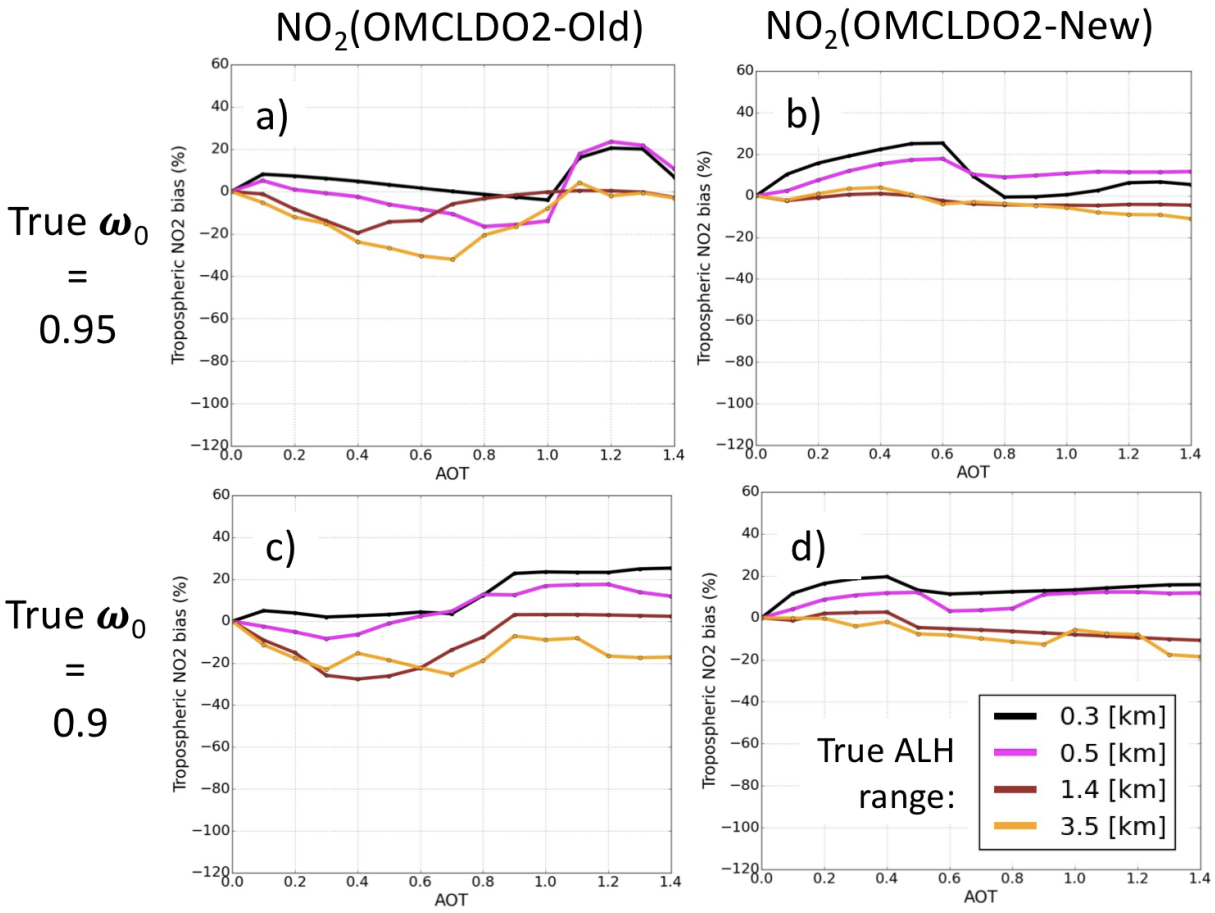

Figure 2. Relative $N^{v}_{NO_2}$ biases after application of the implicit aerosol correction as a function of true aerosol optical thickness (AOT) τ(550 nm) and based on synthetic cases including different true ALH, surface albedo = 0.05, $\mu_0 = 25^\circ$, $\mu = 25^\circ$, and a typical TM5 NO_2 vertical profile for 1st of July, 2006 at 12:00 pm over China (van Noije et al., 2014; Chimot et al., 2016). True aerosol properties are defined by α = 1.5, ω_0 = 0.95 or 0.9 and g = 0.7. Implicit aerosol correction is derived from the retrievals given by OMCLDO2-Old or OMCLDO2-New which, among other elements, includes the new OMI cloud LUT with a higher sampling (see Sect. 2.2 and Tab. 1): **(a)** Relative $N^{v}_{NO_2}$ bias resulting from OMCLDO2-Old, true ω_0 = 0.95, **(b)** Relative $N^{v}_{NO_2}$ resulting from OMCLDO2-New, true ω_0 = 0.95, **(c)** Relative $N^{v}_{NO_2}$ bias resulting from OMCLDO2-Old, true ω_0 = 0.9, **(d)** Relative $N^{v}_{NO_2}$ resulting from OMCLDO2-New, true ω_0 = 0.9.

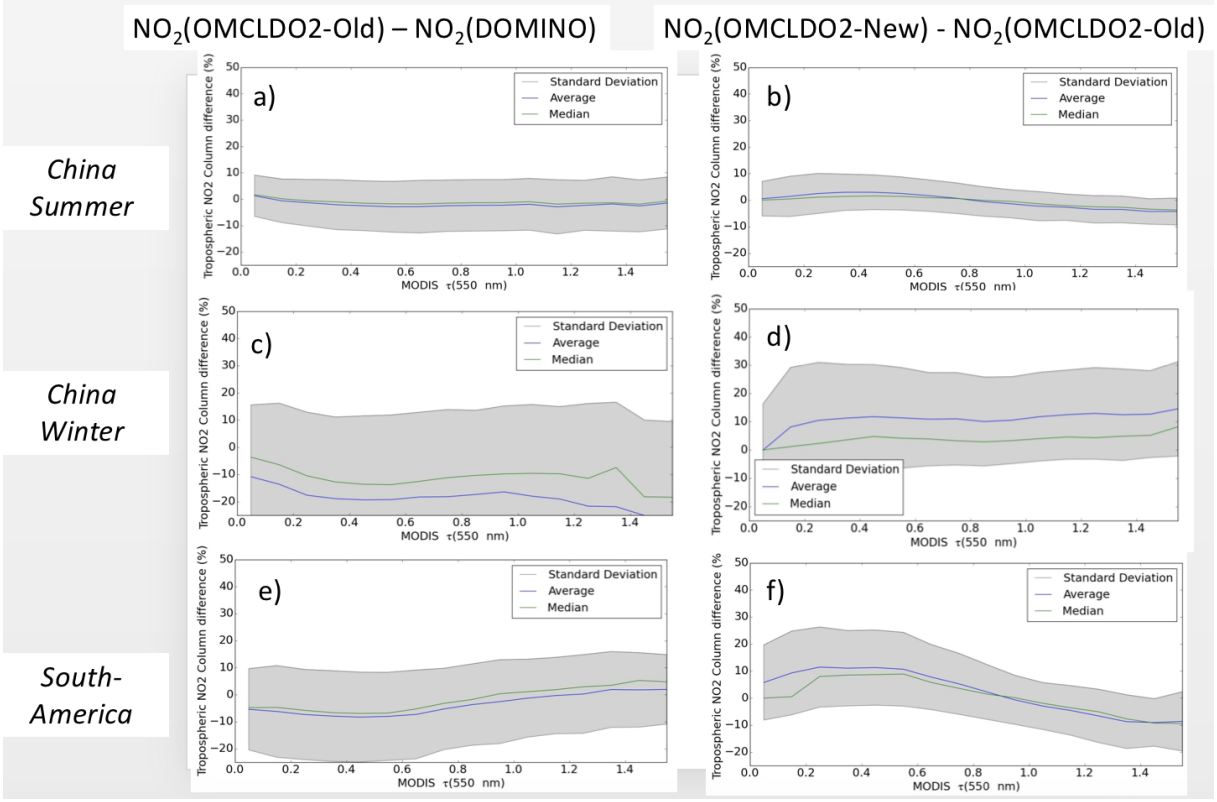

Figure 3. Statistics of relative $N^{\mathrm{v}}_{\mathrm{NO_2}}$ differences in (%) as a function of MODIS τ(550 nm) over China and South America in 2006-2007 due to changes in the applied implicit aerosol correction (cf. Sect. 4.1) from DOMINO to OMCLDO2-Old (with the LER climatology based on a longer time series), and from OMCLDO2-Old to OMCLDO2-New (OMI cloud LUT with a higher sampling): **(a)** China Summer (June-July-August), **(b)** China Winter (December-January-February), **(c)** South America (August-September).

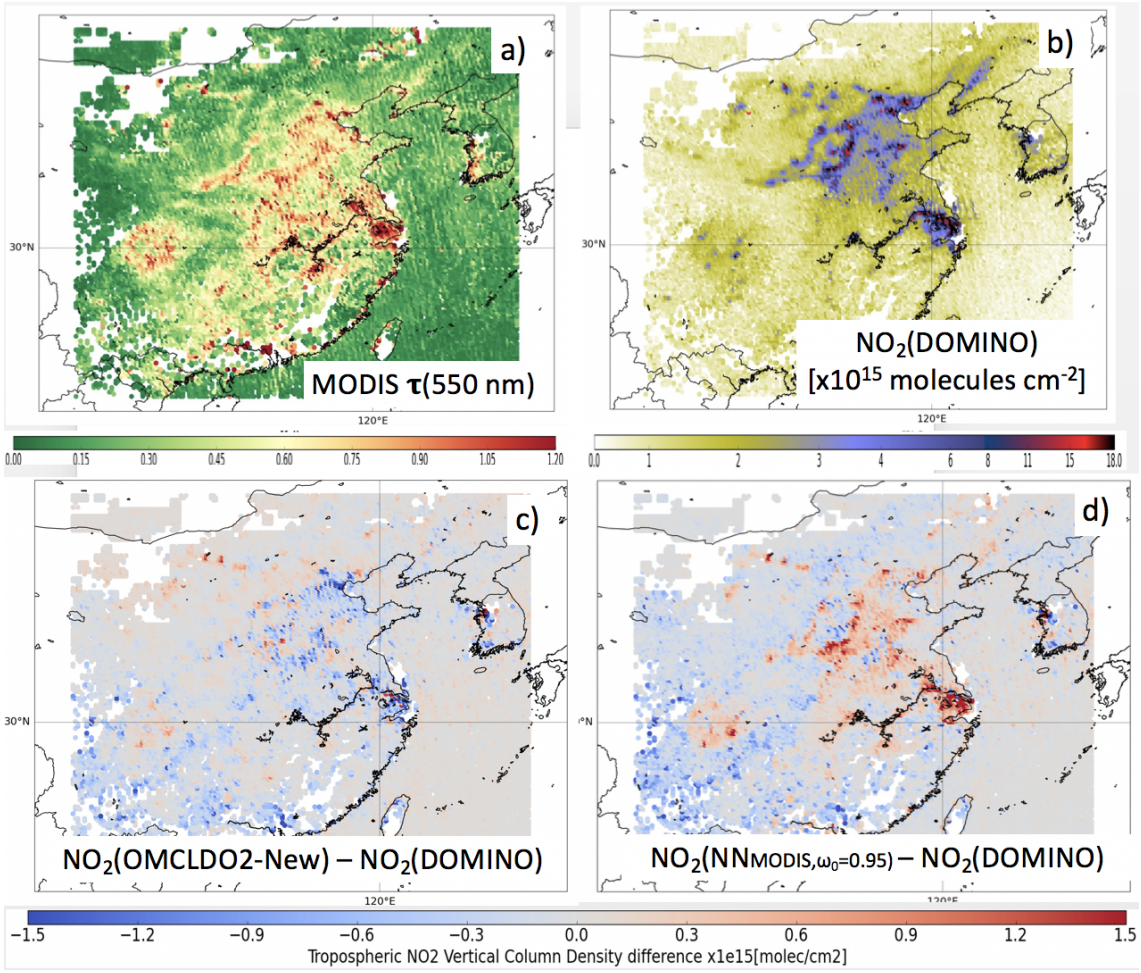

Figure 4. Average maps of MODIS τ(550 nm), OMI DOMINO $N^{v}_{NO_2}$ and differences after applying the implicit (with OMCLDO2-New) or explicit (with $NN_{MODIS,\omega_0=0.95}$) aerosol correction over China in summertime (June-July-August) 2006-2007: **(a)** MODIS τ(550 nm), **(b)** OMI DOMINO $N^{v}_{NO_2}$, **(c)** OMI $N^{v}_{NO_2}$ differences due to changes between OMCLDO2-New and DOMINO implicit aerosol corrections, **(d)** $N^{v}_{NO_2}$ differences between explicit aerosol correction based on the $NN_{MODIS,\omega_0=0.95}$ aerosol parameters (i.e. aerosol forward model assuming ω_0 = 0.95, MODIS τ(550 nm), and retrieved ALH) and implicit aerosol correction implemented in DOMINO.

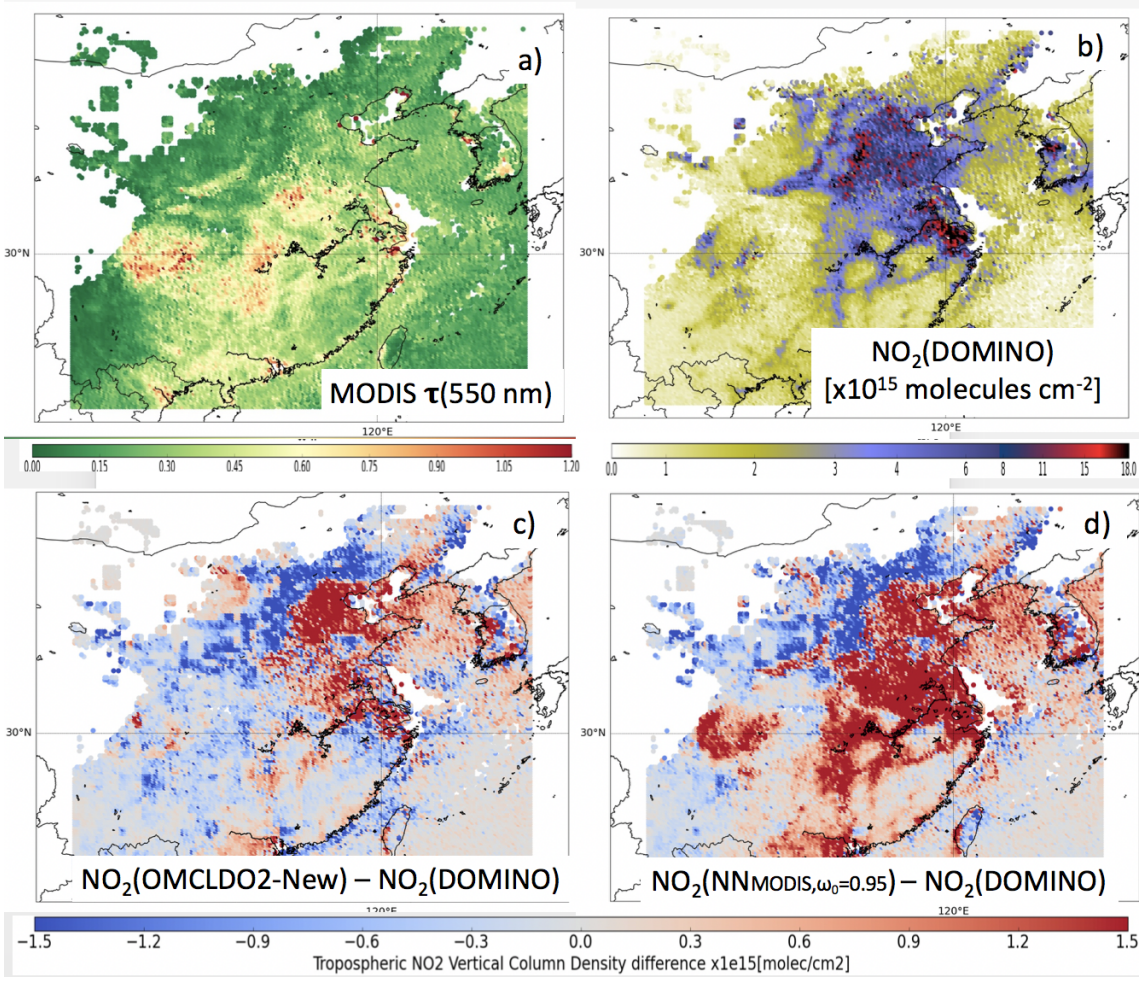

Figure 5. Same as Fig. 4 but over China in wintertime (December-January-February) 2006-2007

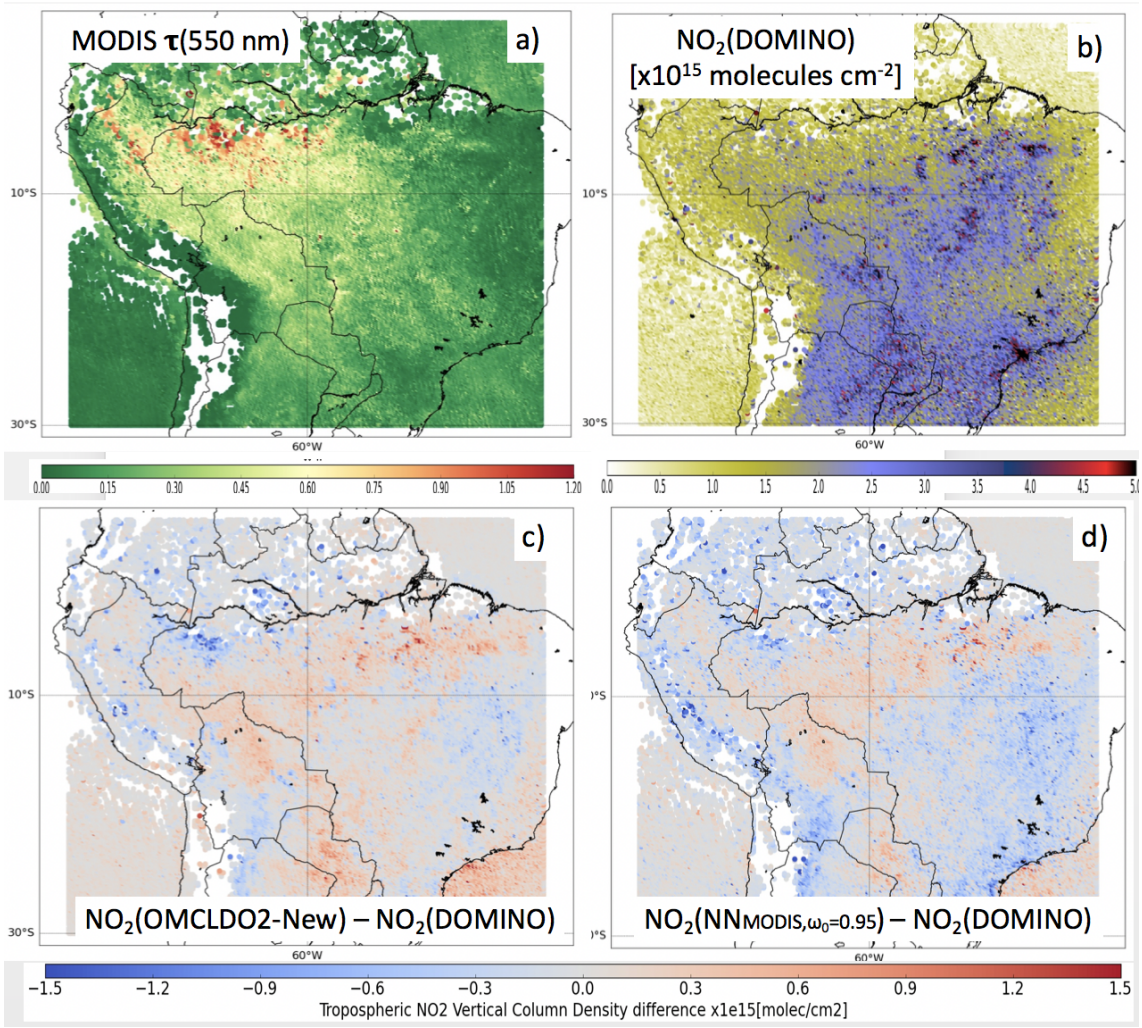

Figure 6. Same as Fig. 4 but over over South America during the biomass burning season (August-September) in 2006-2007

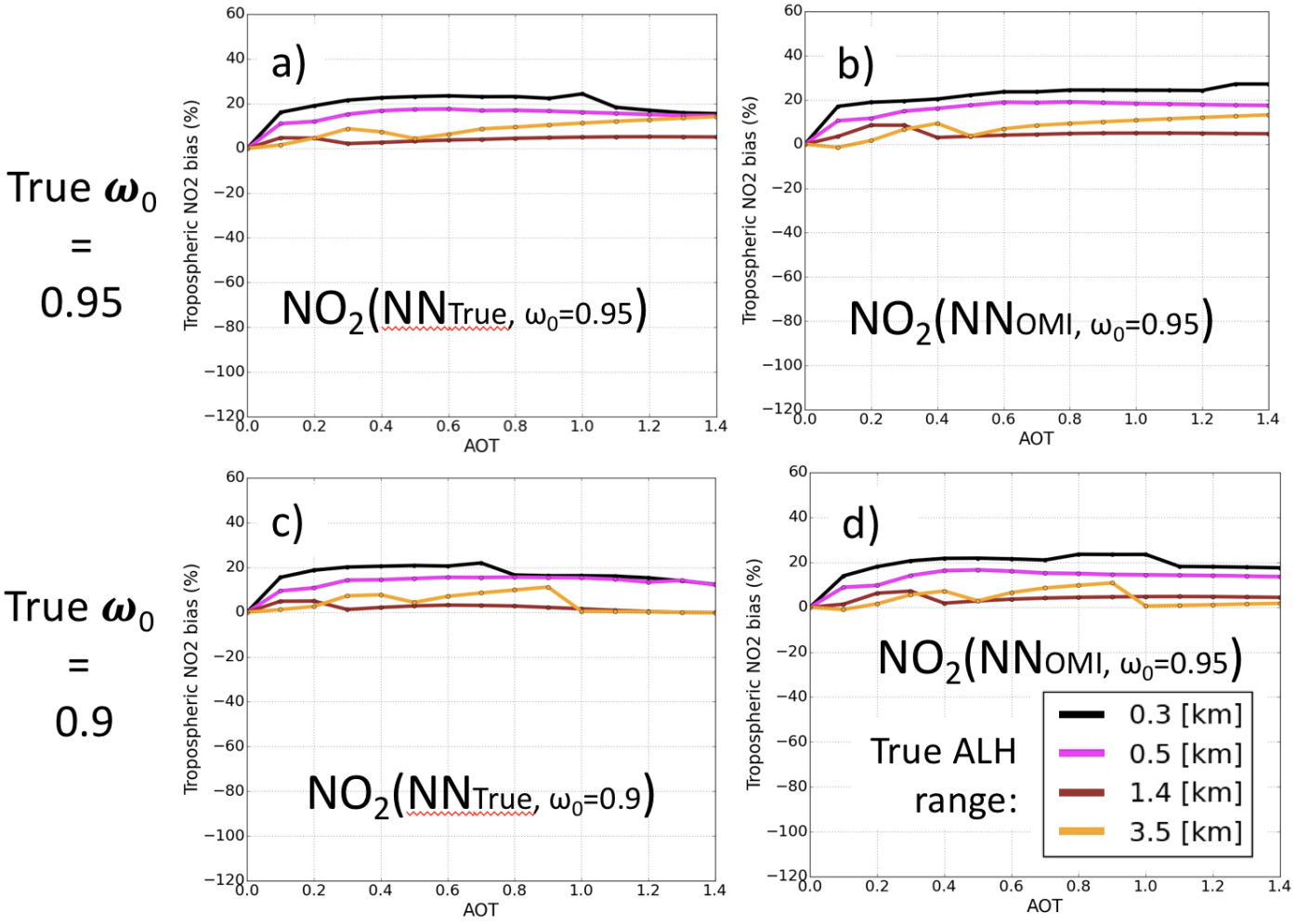

Figure 7. Relative $N^{V}_{NO_2}$ biases after application of the explicit aerosol correction as a function of true aerosol optical thickness (AOT) τ(550 nm) and based on synthetic cases of Fig. 2. No bias is included on ω_0: i.e. true and assumed values are identical: **(a)** True τ and ω_0=0.95, **(b)** Retrieved OMI τ and ω_0=0.95, **(c)** True τ and ω_0=0.9, **(d)** Retrieved OMI τ and ω_0=0.9.

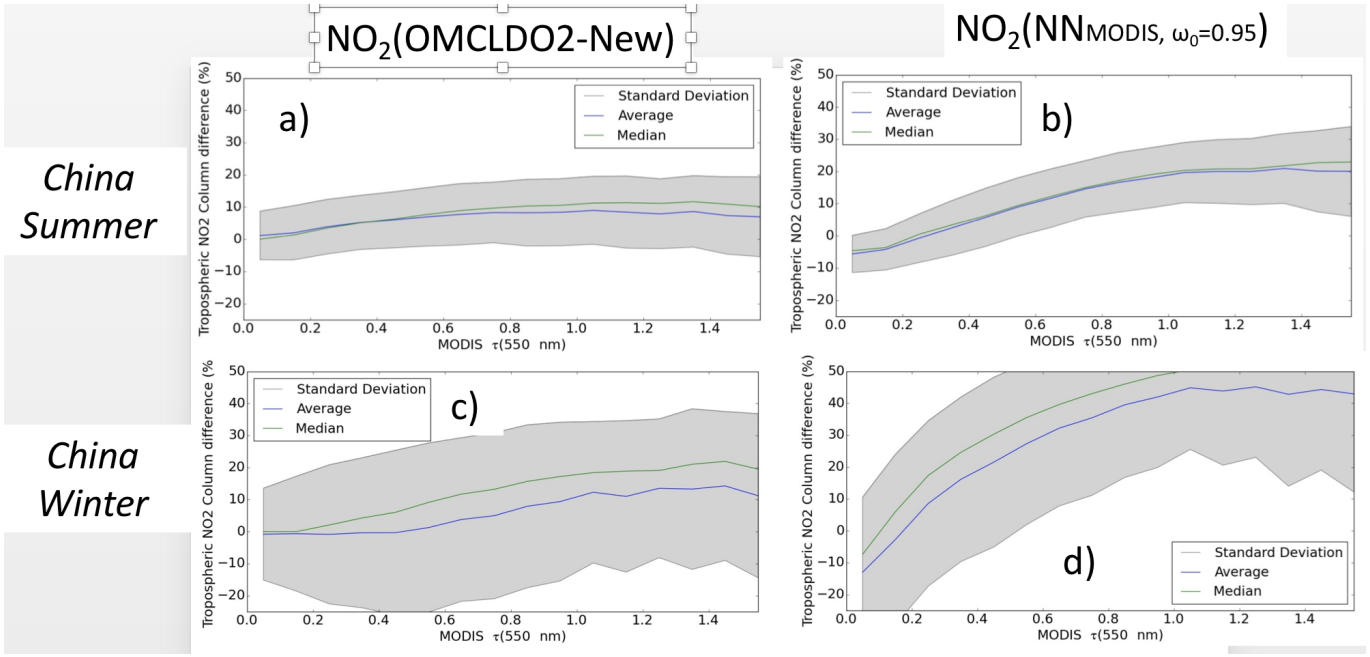

Figure 8. Statistic of relative $N^{V}_{NO_2}$ differences in (%) over China 2006-2007 in Summer (June-July-August) and Winter(December-January-February), after implicit or explicit aerosol correction compared to no aerosol correction (i.e. aerosol-free scene assumption): **(a)** Implicit aerosol correction based on OMCLDO2-New, **(b)** Explicit aerosol correction based on $NN_{MODIS,\omega_0=0.95}$.

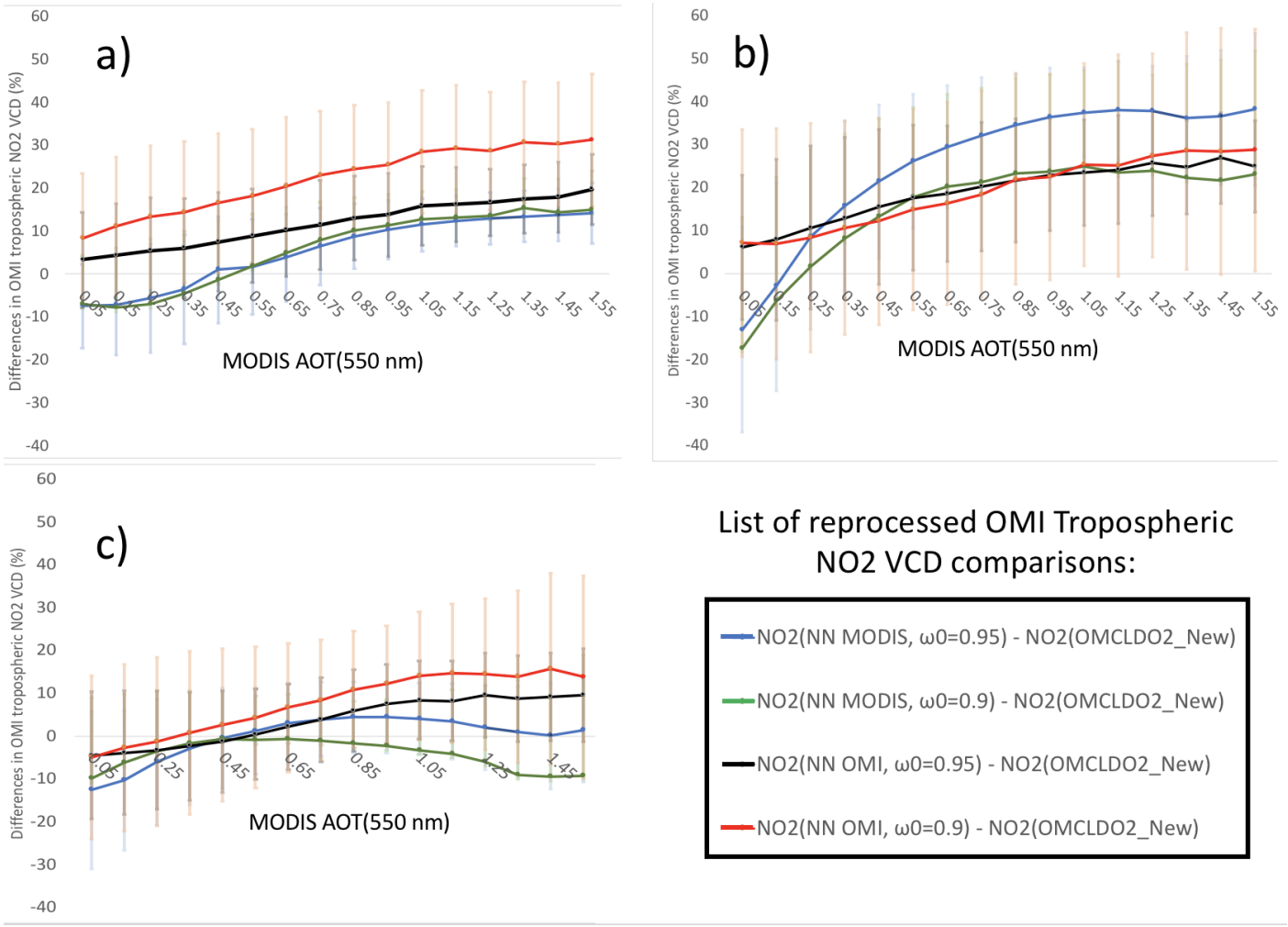

Figure 9. Statistics of relative $N^{\mathrm{v}}_{\mathrm{NO_2}}$ changes in (%) in 2006-2007, due to differences between the different explicit aerosol corrections (see Tab. 1) and the implicit aerosol correction based on OMCLDO2-New (improved effective cloud parameters, up-to-date version): **(a)**: China summertime (June-July-August), **(b)**: China wintertime (December-January-February), **(c)**: South America biomass burning season (August-September).

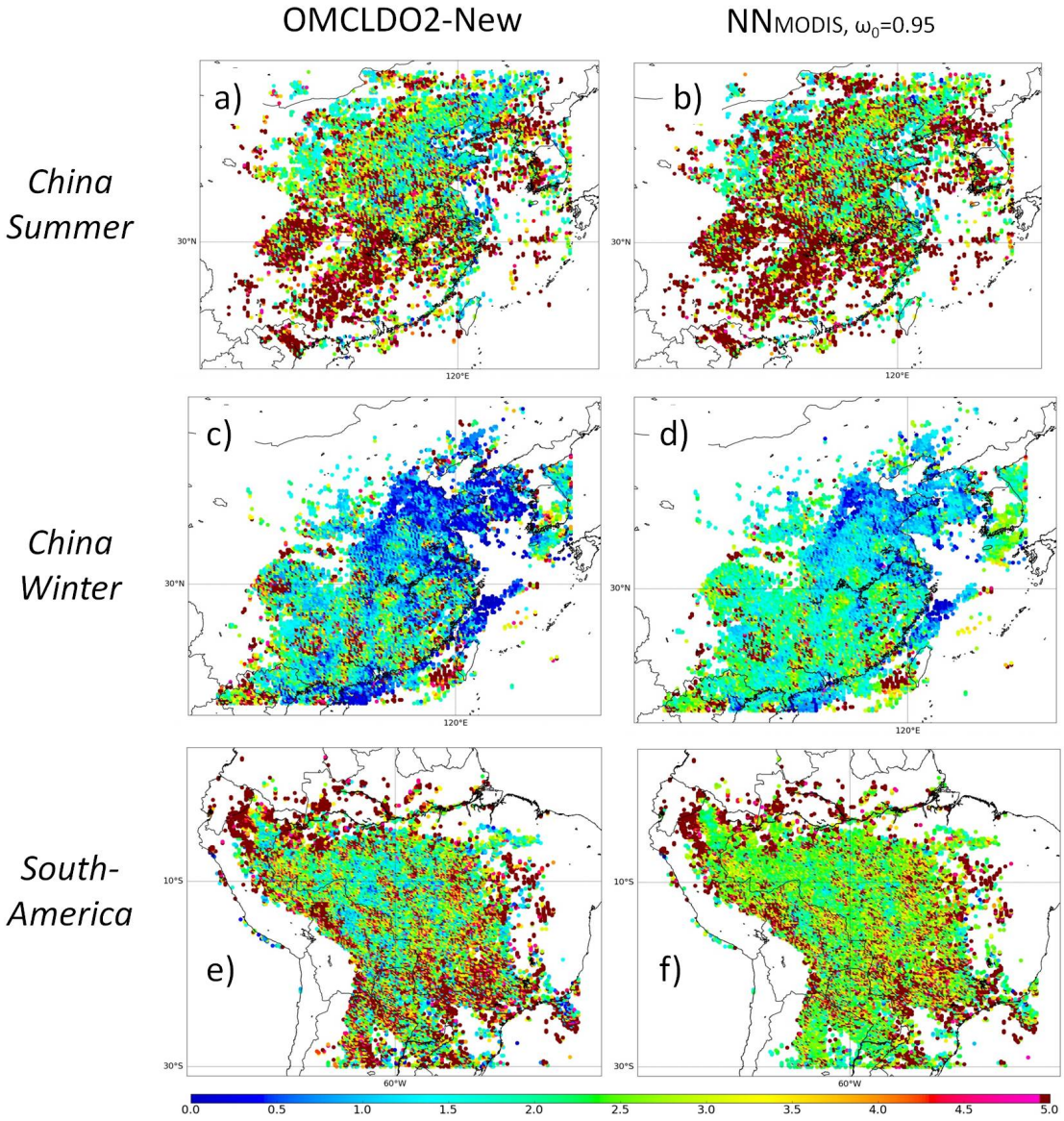

Figure 10. Maps of c_p (converted into cloud height) from OMCLDO2-New and ALH from $NN_{MODIS,\omega_0=0.95}$ in [km] in 2006-2007: **(a)** c_p, China Summer, **(b)** ALH, China Summer, **(c)** c_p, China Winter, **(d)** ALH, China Winter, **(e)** c_p, South America, **(f)** ALH, South America.

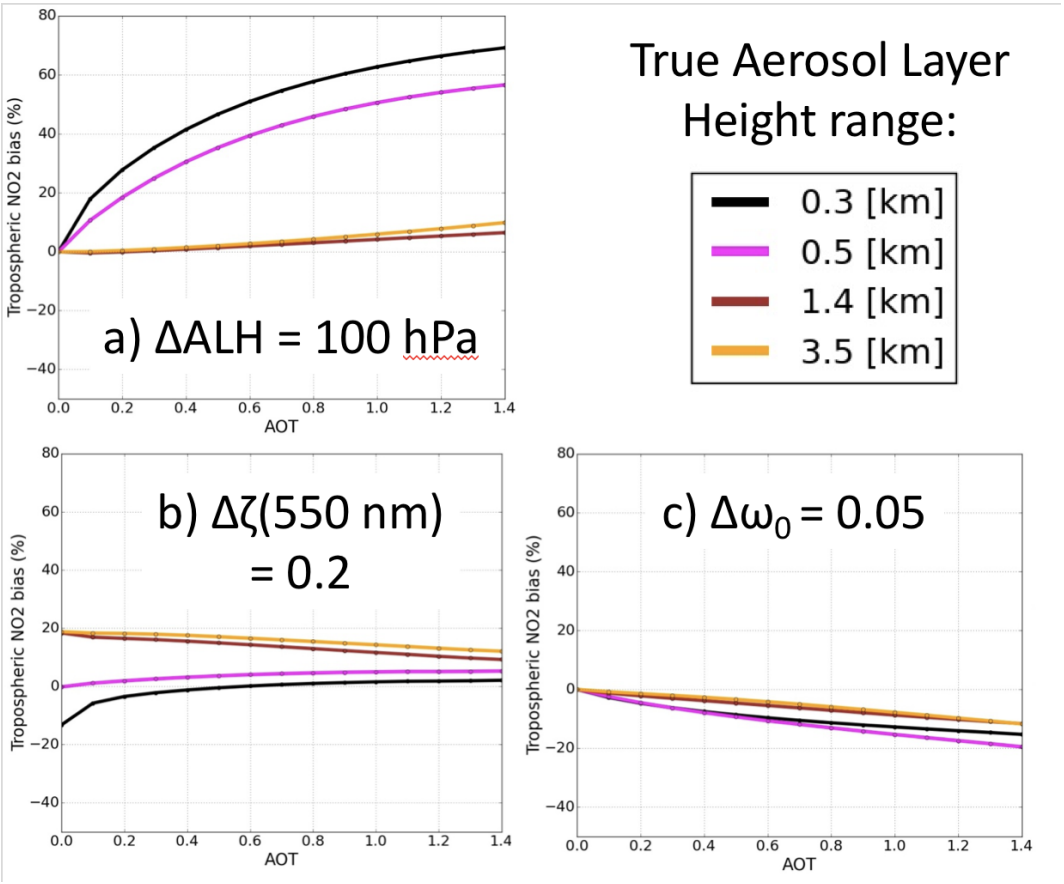

Figure 11. Relative $N^{\mathrm{v}}_{\mathrm{NO_2}}$ biases due to a direct impact of individual aerosol parameter biases on $A^{\mathrm{v}}_{\mathrm{NO_2}}$(439 nm) calculation. Synthetic cases are similar to Fig. 2, with true aerosol ω_0 = 0.9, except a typical mid-latitude winter NO_2 profile is considered instead: **(a)** ALH bias = 100 hPa, **(b)** τ(550 nm) bias = 0.2, **(c)** ω_0 bias = 0.05.

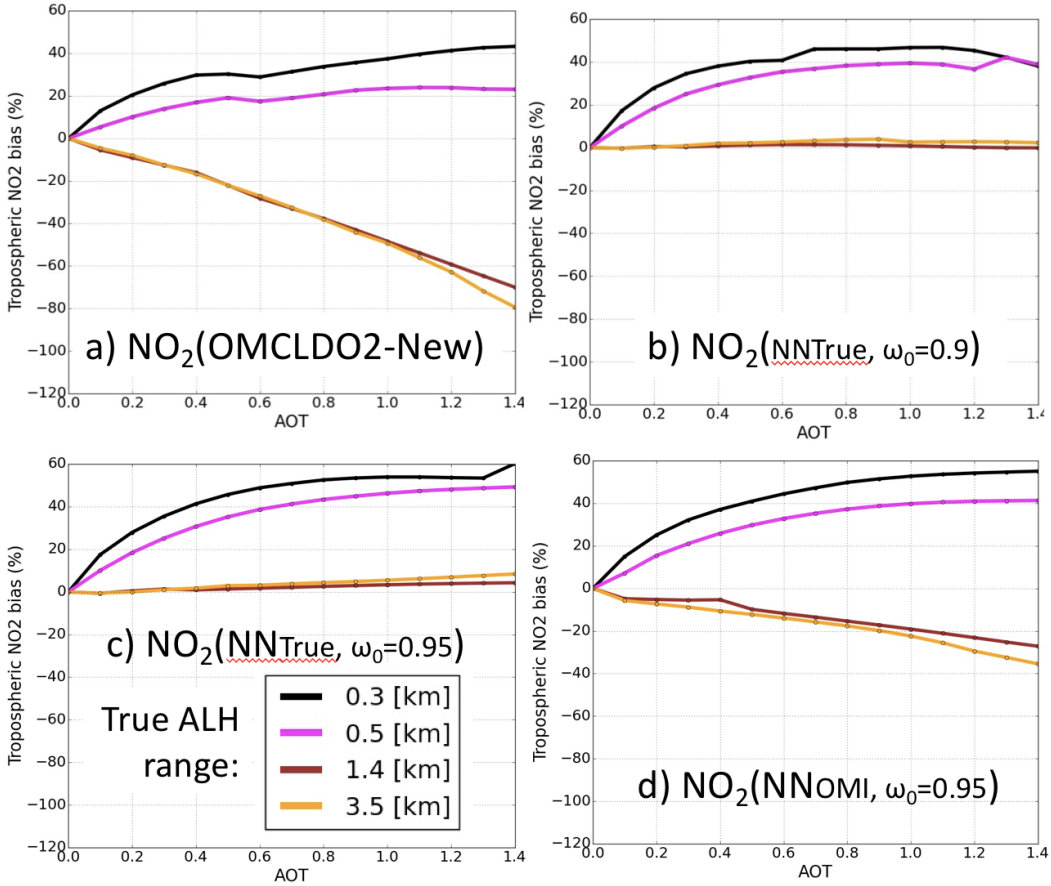

Figure 12. Relative $N^{\mathrm{v}}_{\mathrm{NO_2}}$ biases after application of the implicit or explicit aerosol correction (see Tab. 2) as a function of true aerosol optical thickness (AOT) τ(550 nm). Synthetic cases are similar to Fig. 2 except the summer NO_2 profile was replaced by a typical winter one. Furthermore, only absorbing aerosols with true ω_0=0.9 are considered. Finally, the impact of a bias in the assumed ω_0 through the application of the explicit aerosol correction is illustrated: **(a)** Implicit aerosol correction based on OMCLDO2-New, **(b)** Explicit aerosol correction, true τ and assumed ω_0=0.9, **(c)** Explicit aerosol correction, true τ and assumed ω_0=0.95, **(d)** Explicit aerosol correction, retrieved OMI τ and assumed ω_0=0.95.

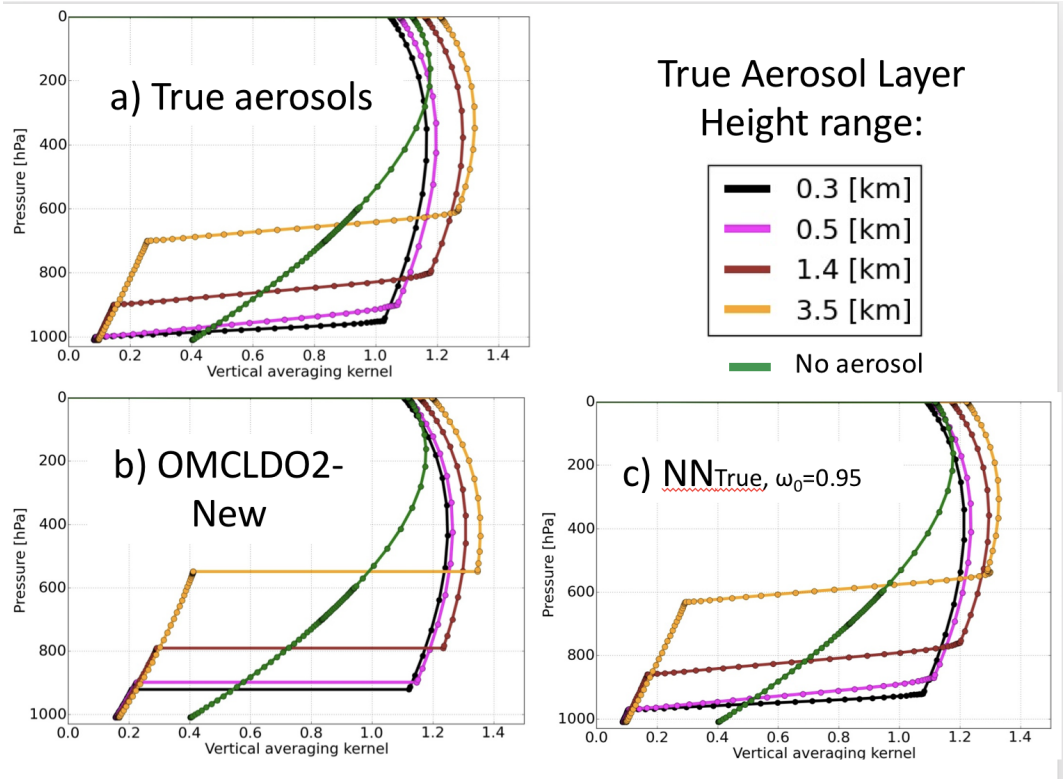

Figure 13. Vertical AK (cf. Sect. 3.2 and Sect. 5.4) based on aerosol τ(550 nm) = 1.0, NO_2 vertical profile of 1st of July, 2006 at 12:00 pm over China. Other conditions are similar to Fig. 2.

Table 1. Summary of the different OMI $N^{\mathrm{v}}_{\mathrm{NO_2}}$ mentionned in this paper, and the configuration of the associated aerosol correction: input OMI Lambertian Equivalent Reflectivity (LER) climatology, OMI cloud look-up table (LUT) for the effective cloud retrievals, Aerosol parameters (see for more details Sect. 2.2, 2.3 and 3)

OMI $N^{\mathrm{v}}_{\mathrm{NO_2}}$ dataset	Aerosol correction	Configuration details
NO_2(DOMINO)	Implicit aerosol correction, OMCLDO2	Coarse OMI cloud LUT
		LER 3-year climatology
		No temperature correction on $N^{\mathrm{s}}_{\mathrm{O_2-O_2}}$
NO_2(OMCLDO2-Old)	Implicit aerosol correction, OMCLDO2	Coarse OMI cloud LUT
		LER 5-year climatology
		Temperature correction on $N^{\mathrm{s}}_{\mathrm{O_2-O_2}}$
NO_2(OMCLDO2-New)	Implicit aerosol correction, OMCLDO2	Fine OMI cloud LUT
		LER 5-year climatology
		Temperature correction on $N^{\mathrm{s}}_{\mathrm{O_2-O_2}}$
$NO_2(NN_{MODIS,\omega_0=0.9})$	Explicit aerosol correction, OMI Aerosol NN	MODIS τ(550 nm), OMI ALH
		LER 5-year climatology
		Assumed ω_0=0.9
		Temperature correction on $N^{\mathrm{s}}_{\mathrm{O_2-O_2}}$
$NO_2(NN_{OMI,\omega_0=0.9})$	Explicit aerosol correction, OMI Aerosol NN	OMI τ(550 nm), OMI ALH
		LER 5-year climatology
		Assumed ω_0=0.9
		Temperature correction on $N^{\mathrm{s}}_{\mathrm{O_2-O_2}}$
$NO_2(NN_{MODIS,\omega_0=0.95})$	Explicit aerosol correction, OMI Aerosol NN	MODIS τ(550 nm), OMI ALH
		Assumed ω_0=0.95
		LER 5-year climatology
		Temperature correction on $N^{\mathrm{s}}_{\mathrm{O_2-O_2}}$
$NO_2(NN_{OMI,\omega_0=0.95})$	Explicit aerosol correction, OMI Aerosol NN	OMI τ(550 nm), OMI ALH
		Assumed ω_0=0.95
		LER 5-year climatology
		Temperature correction on $N^{\mathrm{s}}_{\mathrm{O_2-O_2}}$

Table 2. Summary of the changes in the diverse reprocessing OMI tropospheric NO_2 VCD $N^{v}_{NO_2}$ depending on the applied aerosol correction strategy (see Tab. 1) over all collocated MODIS aerosol scenes (MODIS τ(550 nm) $\geq 0.$). See more analyses in Sect. 4.1-4.2:

Focus on:	Comparison reprocessed NO_2	Region - Season	Changes in $N^{v}_{NO_2}$ in [%] Average $\pm$ Standard Deviation
Implicit correction	NO_2(OMCLDO2-Old) $-$ NO_2(DOMINO)	China - summer	-1.0 ± 9.0
		China - winter	-15.6 ± 29.8
		South America - biomass burning	-6.2 ± 16.0
	NO_2(OMCLDO2-New) $-$ NO_2(OMCLDO2-Old)	China - summer	1.3 ± 6.9
		China - winter	7.9 ± 19.3
		South America - biomass burning	7.9 ± 14.4
	NO_2(OMCLDO2-New) $-$ NO_2(DOMINO)	China - summer	0.4 ± 10.6
		China - winter	-4.0 ± 26.8
		South America - biomass burning	3.1 ± 17.3
. Explicit correction	$NO_2(NN_{MODIS,\omega_0=0.95})$ $-$ NO_2(OMCLDO2-New)	China - summer	-2.9 ± 12.5
		China - winter	6.8 ± 26.1
		South America - biomass burning	-8.1 ± 16.8
	$NO_2(NN_{MODIS,\omega_0=0.9})$ $-$ $NO_2(NN_{MODIS,\omega_0=0.95})$	China - summer	-0.2 ± 7.8
		China - winter	-8.2 ± 22.3
		South America - biomass burning	1.3 ± 8.7
	$NO_2(NN_{OMI,\omega_0=0.95})$ $-$ NO_2(OMCLDO2-New)	China - summer	6.5 ± 11.9
		China - winter	11.2 ± 18.4
		South America - biomass burning	-3.0 ± 14.0
	$NO_2(NN_{OMI,\omega_0=0.9})$ $-$ $NO_2(NN_{OMI,\omega_0=0.95})$	China - summer	8.5 ± 13.7
		China - winter	-1.9 ± 24.3
		South America - biomass burning	1.0 ± 14.6